RI9172

Bureau of Mines Report of Investigations/1988

Computer-Assisted Mine Design Procedures for Longwall Mining

By N. P. Kripakov, L. A. Beckett, D. A. Donato, and J. S. Durr

UNITED STATES DEPARTMENT OF THE INTERIOR

Report of Investigations 9172

Computer-Assisted Mine Design Procedures for Longwall Mining

By N. P. Kripakov, L. A. Beckett, D. A. Donato, and J. S. Durr

UNITED STATES DEPARTMENT OF THE INTERIOR
Donald Paul Hodel, Secretary

BUREAU OF MINES
T S Ary, Director

Library of Congress Cataloging in Publication Data:

Computer-assisted mine design procedures for longwall mining.

(Report of investigations ; 9172)

Bibliography: p. 33-36.

Supt. of Docs. no.: I 28.23:9172.

1. Longwall mining--Mine design. I. Kripakov, Nicholas P. II. Series: Report of investigations (United States. Bureau of Mines) ; 9172.

TN23.U43 [TN275] 622'.334 87-600435

CONTENTS

ILLUSTRATIONS

ILLUSTRATIONS--Continued

TABLES

UNIT OF MEASURE ABBREVIATIONS USED IN THIS REPORT

deg	degree	lb/in	pound per inch
ft	foot	pct	percent
ft^3	cubic foot	psi	pound per square inch
ft/ft	foot per foot	psi/ft	pound per square inch per foot
GPa	gigapascal	psi/psi	pound per square inch per pound per square inch
in^2	square inch	st	short ton
in/in	inch per inch		
lb	pound		

COMPUTER-ASSISTED MINE DESIGN PROCEDURES FOR LONGWALL MINING

By N. P. Kripakov,[1] L. A. Beckett,[1] D. A. Donato,[1] and J. S. Durr[2]

ABSTRACT

The Bureau of Mines has developed a unique new mine design procedure to determine the changing static load distributions imposed on underground support structures during the mining cycle. The procedure reduces the complexities associated with analyzing a three-dimensional problem. A combination of the multiple-seam displacement-discontinuity model and a two-dimensional finite-element window model produces refined results for a specific area of interest by assuming displacement compatibility between models. Input to the procedure includes the geometry of mined-out areas in up to two adjacent seams, the rock mass characteristics of the surrounding geology, the in situ stress conditions, and the mining sequence. The displacement-discontinuity program calculates expected loadings for mine structures affected by the mining cycle and/or by overlying or underlying seams. Pseudoelastic finite-element analysis using a yield-factor approach determines the stability of coal pillars by simulating the degree and extent of progressive rib failure and subsequent load transfer.

Application of the procedure is demonstrated on a field problem. Induced stress changes predicted from the numerical model analysis are in reasonably good agreement with stress measurements obtained from an instrumented chain pillar affected by remnant workings in an upper seam.

[1]Mining engineer.
[2]Engineering technician.
Denver Research Center, Bureau of Mines, Denver, CO.

INTRODUCTION

The design of underground support pillars and entry systems in longwall mining operations is one of the major problems facing coal mine operators in the United States today. One important factor in designing a mine plan for a retreat longwall mining operation is estimating the loads imposed on various portions of the underground support structure during the mining sequence, from initial entry development through complete extraction of adjacent panels. This information is critical to designing a safe and efficient gateroad and barrier pillar support system. Improper design of barrier pillars protecting main entries can be disastrous to a mining operation should the barrier pillar fail. Knowledge of expected rear abutment pressures in or behind the gob zone can reduce the probability of ground control problems in the bleeder entries through proper pillar design. Chain pillars separating two adjacent longwall panels must be designed to assure competent underground entries during retreat mining of the first longwall panel and to protect its headgate entry for use as a tailgate entry for the next longwall panel.

Approximately 56 pct of the country's 283-billion-st recoverable coal reserves must be mined by underground methods (1).[3] A significant percentage of this coal lies in multiple-seam deposits in close stratigraphic proximity. Of these reserves, more than 65 pct, primarily in the Appalachian Region of the Eastern United States, are situated under less than 1,000 ft of cover (2). It is common practice in the East to mine adjacent coalbeds simultaneously or to mine over or under a previously mined-out coalbed (3). In the Western United States, a substantial portion of coal reserves are located under depths of cover greater than 1,500 ft, making them susceptible to ground control problems such as pillar bounces, roof falls, and floor heave. These problems are magnified when mining over or under old workings. Many current longwall mining operations throughout the United States have experienced localized, yet severe ground control conditions as a result of seam interaction. These problems will continue to grow in importance as operators are forced to open new seams above or below seams currently being mined.

Past mining practice was based primarily on ownership and economics with little regard for the effects of mining on adjacent coalbeds. In many cases, the resulting ground control problems have rendered these adjacent resources unminable, unless methodologies and techniques are developed to provide the mining industry with analytical tools to assist in the layout of rational mining plans. A well-thought-out plan can minimize the safety hazards associated with extracting multiple-seam coal reserves.

The Bureau of Mines is developing theoretical numerical modeling techniques, verified by field data, to assist the mining industry in designing safe and efficient mines for single- and multiple-seam coal mining. The focus of this Bureau research is on providing the industry with new, computer-oriented analytical tools to quickly and efficiently assess the three-dimensional effects of stress concentrations imposed on underground support structures. This report presents a new computer-assisted mine design procedure to aid coal operators in estimating the continuous changes from induced loading imposed on all remaining underground support structures as a function of the mining cycle, taking into consideration the effects of underlying or overlying coal seams.

From a structural aspect, mine design problems should be considered from a large-scale viewpoint. As entries are driven and pillars are formed to support overburden weight, vertical loading throughout an active mining section continually changes in magnitude and direction. Load transfer is highly dependent on structural geology, competency of the strata, and compaction characteristics of the gob. Weight is transferred by a

[3]Underlined numbers in parentheses refer to items in the list of references preceding the appendix.

combined effect of beam bending and arching over openings.

In general, mining extends over an area so large that, for practical reasons, the entire mining area cannot be included in the analysis. In numerical methods such as finite-element and boundary-element procedures, the region excluded from the analysis is replaced by appropriate boundary conditions. However, for multiple-seam mining situations, it is difficult to set such boundary conditions realistically. The general procedure described here considers only a portion of a mine plan, focusing on a designated mine area. Any mining beyond this area is assumed to have a negligible effect on the induced displacements and stresses in the specific areas of interest.

Little documentation exists in the United States on extracting multiple seams using longwall mining methods. With the exception of a few mines already employing longwall, the majority of underground mines have used the room-and-pillar method exclusively, usually with secondary pillar recovery. Extraction of multiple seams in sequence from the top down reduces harmful interaction effects somewhat; however, the uppermost seams may be lower in quality or thinner or may yield a lower rate of return such that this practice is not economically viable to mine operators, who are likely to extract the best quality seams first. Enlightened mine operators, who wish to maximize long-term benefits and not sterilize future reserves, are more likely to use improved mining methods and take advantage of the latest innovative mine design procedures.

During the early 1970's, Jacobi and Everling (4) developed a numerical analysis procedure to analyze seam interaction problems in West German coal mines. The procedure was based on a single degree-of-freedom finite-element approach. The method has certain limitations in that no lateral displacement of the nodal points is allowed. Therefore, the calculated stress distribution is a direct function of the axial (vertical) stiffness only. The potential bending stiffness of the interburden layers is not accounted for, thereby distorting the accuracy of the final load distribution. During the early 1980's, Pariseau (5) and Su (6) each used finite-element models to further analyze the interaction of multiple-seam mining; however, neither author dealt specifically with the longwall mining method.

Pillar design in this country is based primarily on foreign literature, rule-of-thumb estimates, and practical experience, and no single accepted method for pillar design exists today that is suitable for all types of geological environments. What works in one particular mine may not be successful in another mine with its own unique conditions. Some mining companies use yield pillars to protect their gateroads, other mines use stable pillars, and some use a combination of both (7).

Conventional methods of estimating pillar loading do not incorporate effects of unsymmetrical geometric configurations, mining sequence, and seam interaction. Numerous design formulas (8-11) exist that relate the width-height ratio of laboratory-tested rock samples to allowable pillar load, but most of these consider a pillar in an isolated sense, acting independently of adjacent pillars or of other support structures; the interacting effects of the roof and floor on pillar integrity are not always considered. Wilson's confined core pillar design method (12-13) attempts to include effects of confinement and extent of pillar rib yielding as a function of both the effective overburden depth and the relative strength of roof and floor. Babcock (14-16) points out the importance of constraint in pillar design. Panek (17) proposes a pillar design equation based on the theory of similitude, in which the physical properties of the roof, floor, coal, and steel loading platens are used with laboratory model pillars of the same geometry as the mine pillars. Carr and Serata's stress control method (7, 18) shows promise for controlling floor heave in development entries for a future longwall panel, but the method has yet to be field-verified for a complete mining cycle.

ACKNOWLEDGMENTS

The authors wish to thank the following individuals for their contributions to the work reported herein:

Meng-Cherng Sun, mining engineer, Bureau of Mines, Denver Research Center (now with the U.S. Geological Survey), who developed the preprocessing software for the ADINA finite-element computer program; Karl Dise, civil engineer, Bureau of Mines, Denver Research Center (now with the U.S. Department of the Interior's Bureau of Reclamation), who installed and developed mesh-generating software for the original version of the MULSIM computer program to be compatible with the Tektronix 4054 Graphics Computer System;[4] Rudy Madrid, systems engineer for Electronics Data Systems Corp. (EDS), on contract to the Bureau of Mines Automatic Data Processing (ADP) Division in Denver, for providing programming assistance to expand and restructure the MULSIM computer program and for developing postprocessing graphics for MULSIM output; James R. Albin, operations research analyst, Bureau of Mines, Denver Research Center, who developed postprocessing software for ADINA output; Matthew DeMarco and John Koehler, mining engineers, Bureau of Mines, Denver Research Center, for designing, installing, and monitoring the field instrumentation in support of this study.

METHOD OF ANALYSIS

The basic theoretical approach presented in this report is conceptually illustrated in figure 1. The procedure, in effect, reduces a complex three-dimensional problem to two dimensions. For each simulated face position, two distinct and separate phases of computer modeling are performed. The first phase of computer modeling considers a designated portion of the mine layout in plan view. This phase uses the displacement-discontinuity approach to determine the overall large-scale induced stresses imposed on all remaining in-seam support structures. It also determines all induced in-seam displacement values and all additional displacement values at designated off-seam locations for a particular face position. Load effects include overburden weight, load concentrations resulting from nearby mined-out workings in overlying or underlying seams, and lateral load transfer effects resulting from adjacent mined-out gob zones in the longwall panels. A gob model developed specifically for this procedure is used to estimate the vertical support capacity of the caved zone behind a longwall face.

The second phase of computer modeling isolates and studies a specific area of interest in greater detail with a vertical section view. This vertical section is represented by a two-dimensional finite-element window model. Computed displacements from the displacement-discontinuity model are used as input values to the finite-element model at common interface points between models. The finite-element model is assumed to behave elastically under plane-strain conditions. For the sake of simplicity and practicality, it is assumed that the out-of-plane displacements obtained from the displacement-discontinuity model have a negligible effect on the final results obtained from the finite-element plane-strain analysis, and, in this sense, displacement continuity or compatibility is maintained between the two modeling approaches.

Stress output from the finite-element model is compared with a two-dimensional Mohr-Coulomb failure criterion. The stability of coal pillars is assessed using an iterative yield-factor approach. The criterion for stability is based on the degree and extent of progressive pillar rib failure predicted with the finite-element model. The degree of failure, referred to in the text as the "yield factor," is defined as the relative level of competency of the rock mass to support

[4]Reference to specific products does not imply endorsement by the Bureau of Mines.

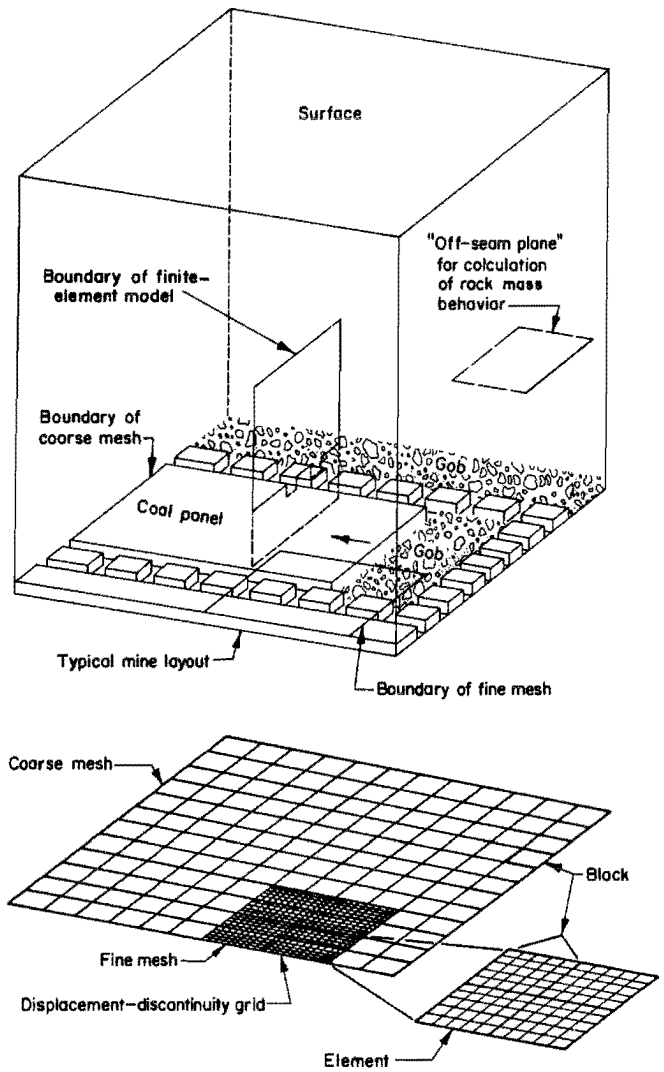

FIGURE 1.—Illustration of theoretical approach.

load before and after failure. The extent of failure is defined as the lateral distance into the coal pillar rib that some degree of weakening or deterioration has occurred.

A modified version of program MULSIM (19) is used for the first phase of computer modeling to determine overall applied vertical loading imposed onto the remaining underground support structure as a function of mining sequence. This computer code is based on a variation of the boundary-element method called the displacement-discontinuity approach, developed originally by Crouch and Fairhurst (20). Application of this technique is based on a mathematical model in which a tabular seam is represented as a single plane in a homogeneous, isotropic elastic medium. Multiple seams are modeled as a set of planes representing the seams at different levels. The Bureau-modified version of the MULSIM program is called MULSIM/BM and is described in the following section of this report.

The mining area represented in the MULSIM/BM model is discretized in small, rectangular blocks and elements as illustrated in figure 1. Each of these elements corresponds to either an unmined or a mined portion of a seam, and for each element, the values of the stress components and displacement components are considered to be uniform. The term "displacement discontinuity" refers to the abrupt changes that occur at the element boundaries. For each element, stresses and roof displacements are calculated by summing the interactive effects of element displacements throughout the model. The effective stiffness of the overall model is calculated by using the intraseam and interseam elastic influence coefficients based on the model geometry and the rock mass material properties. The elastic response of the element itself to the applied stresses depends on the element material properties. Each element is assigned an alphanumeric value indicating the mining status and the material property set to be used for the element. The mining status indicates that a zone in the model is either mined out, unmined, caved, or in a yielded state. MULSIM/BM incorporates a gob material model and can define up to 26 different material property sets.

Displacement values obtained from MULSIM/BM are used as a separate and distinct boundary loading condition for a two-dimensional finite-element model, as conceptually illustrated in figure 1. A general-purpose finite-element computer program, ADINA (21), is used to calculate all internal nodal displacements and stresses in the vertical section window model.

Utilizing a modified version of procedures developed by the Bureau to simulate progressive rock failure (22-24), a relationship between postfailure strength and stiffness is established and employed in a step-by-step iterative procedure to determine analytically the continually

changing degree and extent of failure through a pillar cross section, caused by both field and mining-induced stresses. Material properties are modified after each iteration by a factor proportional to an updated element safety factor until an equilibrium state is reached where the new material property values do not change significantly. The analysis is terminated at this point, and the results are evaluated.

DESCRIPTION OF MULSIM/BM COMPUTER PROGRAM

PROGRAM HISTORY

A subvariation of the boundary-element method called the three-dimensional displacement-discontinuity approach was originally incorporated into a mine structural analysis computer program by Crouch and Fairhurst (20). In this approach, the mine plan for each seam is specified as a grid in plan view; the program then calculates the resulting three-dimensional stresses and ground deformations that result from mining. Sinha (19) expanded upon the theory of the approach in three computer programs, one of which, MULSIM, was designed to analyze situations of parallel multiple coal seams. During 1984-85, the Bureau upgraded and completely restructured the MULSIM program into the MULSIM/BM program.

Bureau IC 9168 (25) documents the improvements incorporated in the MULSIM/BM program and provides a complete user's guide. For detailed explanation of the mathematical theories incorporated within MULSIM/BM, the reader is referred to the previous literature (19-20, 25-27).

CAPABILITIES

The following capabilities of the MULSIM/BM program (25, 28) were carried over from the original MULSIM program: MULSIM/BM is designed for analysis of mine designs in single coal seams or in parallel multiple coal seams. The seams can dip at any angle and lie at any orientation to the virgin principal stress field. As shown in figure 1, the current mining situation is specified to the program in terms of a grid of blocks containing elements; the program then calculates the resulting seam stresses and closures for each element and block. By specifying "off-seam planes," stresses and rock mass deformations are also available for desired points in the surrounding rock mass. The rock mass itself is assumed to be a homogeneous, isotropic, infinite elastic body.

New features of MULSIM/BM include--

1. Ability to specify up to 26 different material property sets.
2. Ability to distinguish between original seam materials (coal) and inserted materials such as gob, pack walls, or cribs. The inserted material model (or gob model) uses a linear stress-strain relationship with zero stress at zero seam closure.
3. Ability to model a larger area with a grid of undivided or "coarse-mesh" blocks.
4. Ability to specify extraction ratios for the undivided or "coarse-mesh" blocks.

In addition, a mesh-generator program was written to complement the MULSIM/BM program.

ANALYTICAL USES

One application for the MULSIM/BM computer program is predicting the continuous change in loading, in plan view, imposed on a row of coal mine chain pillars and/or artificial supports such as pack walls, backfill, cribs, or steel supports for any stage of mining. Another use is to predict the magnitude of potential ground control problems caused by stress concentrations transferred from adjacent mined seams. If the mine plan under consideration is based upon similar operations elsewhere or if the in situ stress field or material property conditions are not fully known, the program can analyze the effects of a different seam dip, different geomechanical properties, and/or a

different in situ stress field. The program is very useful for evaluating the changes in applied loading on all support structure as a function of mining sequence (25, 28).

The program is best suited to situations where strata properties are relatively uniform and where localized geological discontinuities such as rolls, kettlebottoms, or faults do not strongly affect the problem. If local discontinuities or property variations are significant, then a two- or three-dimensional finite-element or discrete-element analysis may be a better approach.

DESCRIPTION OF ADINA COMPUTER PROGRAM

Program ADINA (Automatic Dynamic Incremental Nonlinear Analysis) (21) is a general-purpose finite-element program used for static and dynamic displacement and stress analysis of solids, structures, and fluid structure systems. ADINA is an extension of programs NONSAP (29) and ADINA/BM (30), developed under earlier Bureau contracts. ADINA is capable of analyzing structural systems using combinations of different finite elements. However, for rock-mechanics-related mine design problems, the following element types are used: two-dimensional plane stress, plane strain, and axisymmetric quadrilateral elements; three-dimensional truss elements; three-dimensional solid elements; and three-dimensional beam elements.

Program ADINA can be employed to perform linear and nonlinear analysis. However, the Bureau has, in most cases, limited its research to simple, linear-elastic continuum analysis because of a general lack of availability of appropriate, field-verified, more complex material models. Current solution capabilities of existing nonlinear material models in ADINA are limited in their ability to properly simulate the constitutive relationships of most rock materials. The material models presently available in ADINA can describe only adequately the initial linear-elastic portion of the complete stress-strain curve of coal. None of the material models available in the program accounts for an unloading ratio (strain-softening) in elements after failure. This unloading ratio reflects the well-known postpeak strength of rock under triaxial stress states at different locations from an opening. Since many mine structures allow for, or are subject to, partial yielding of the coal, the analytical range using present models is limited; therefore, the Bureau devised an alternative numerical failure procedure (24) to represent this range of behavior.

The version of ADINA used for this study and its associated preprocessing and postprocessing graphics software are compatible with most major mainframe computers and some minicomputer systems.

DESCRIPTION OF NUMERICAL MODELING PROCEDURE

GENERAL PROCEDURE

A general description of the steps necessary to implement this modeling procedure is outlined in figure 2. For each face position, as conceptually illustrated in figure 1, output displacements from MULSIM/BM are used as a boundary condition set for a series of finite-element model runs. The finite-element model runs simulate progressive partial failure of the chain pillar under the load conditions imposed by each succeeding boundary displacement set. The process requires comparison of the computed stresses in each coal element with a Mohr-Coulomb strength criterion for failure stress after each finite-element run. If the computed element stress exceeds the element failure stress, then the material property number (which includes Young's modulus, Poisson's ratio, and compressive strength) for that element is changed for the succeeding finite-element run to a property number with less strength and stiffness, thus simulating progressive partial failure of the element. In principle, this procedure should continue until all elements reach an equilibrium in which the computed

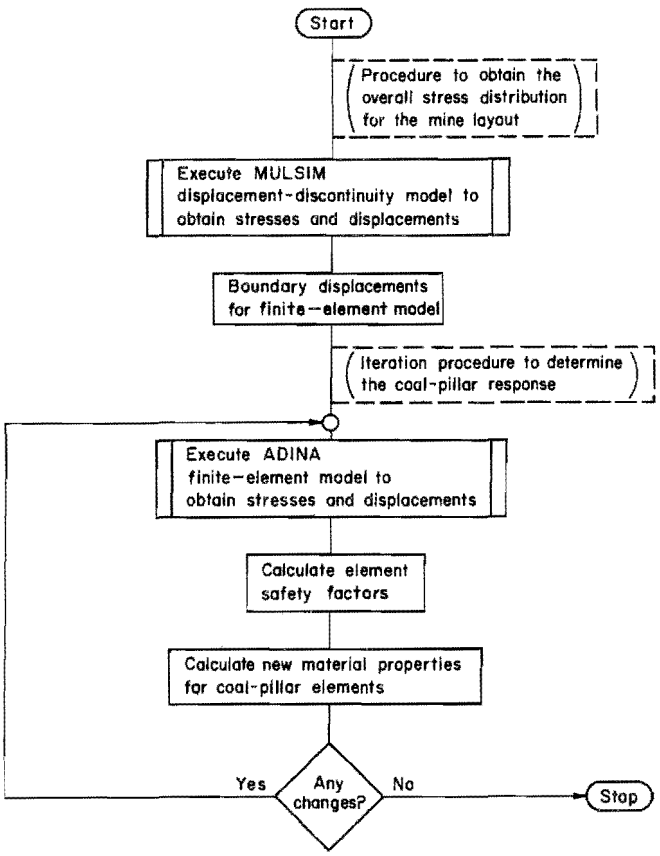

FIGURE 2.–General step-by-step flow chart of procedure.

element stresses do not exceed the failure stresses for the current material strength of that element.

APPLIED STRESS

The steps required to conduct a detailed structural analysis on an isolated vertical cross section of a finite-element window model are illustrated in chronological order in figure 3.

A two-dimensional finite-element mesh is first generated so that the dimensions of the outside boundary node locations are compatible with the designated off-seam locations specified in the displacement-discontinuity model. For the case of a typical longwall entry system, a portion of a typical mesh configuration is illustrated in figure 3*A*. Pertinent input parameters include geometry, geology, rock properties, and the in-plane boundary displacements obtained from the displacement-discontinuity model. It should be noted that this procedure is set up to be compatible with the ADINA code input-output formats. ADINA format requires that two-dimensional models be set up in the Y-Z plane with the X-direction being out of plane, as shown in figure 3*A*.

Once the generated mesh is properly checked out and verified, the appropriate boundary displacements are imposed, and the model is executed to determine the displacements and stresses throughout the total structure. Displacement output is printed out at the nodal points of each element (fig. 3*B*). There is an option in ADINA to print out stresses at nodal points and/or integration points as shown in figure 3*B*. This procedure is set up to print out stresses at the integration points, so that a better estimate of the average stress acting through the element in the region of interest can be achieved.

In general, if good correlation can be achieved between predicted results and actual field measurements of displacements, more credibility can be attached to the stress output. It is easier to monitor displacements (convergence) in the field than to monitor absolute stress.

Stresses are printed out in both the global reference coordinate system (fig. 3*C*) and the principal stress directions (fig. 3*D*) at each integration point in each element. The applied normal and shear stresses (fig. 3*E*) are related to the principal stresses by the relationships

$$\sigma_n = \frac{\sigma_{max} + \sigma_{min}}{2} + \frac{\sigma_{max} - \sigma_{min}}{2} \cos 2\theta. \quad (1)$$

and

$$\tau_n = -\frac{\sigma_{max} - \sigma_{min}}{2} \sin 2\theta \ (31). \quad (2)$$

These applied stress levels are then compared against a strength criterion to determine if localized failure is predicted to occur.

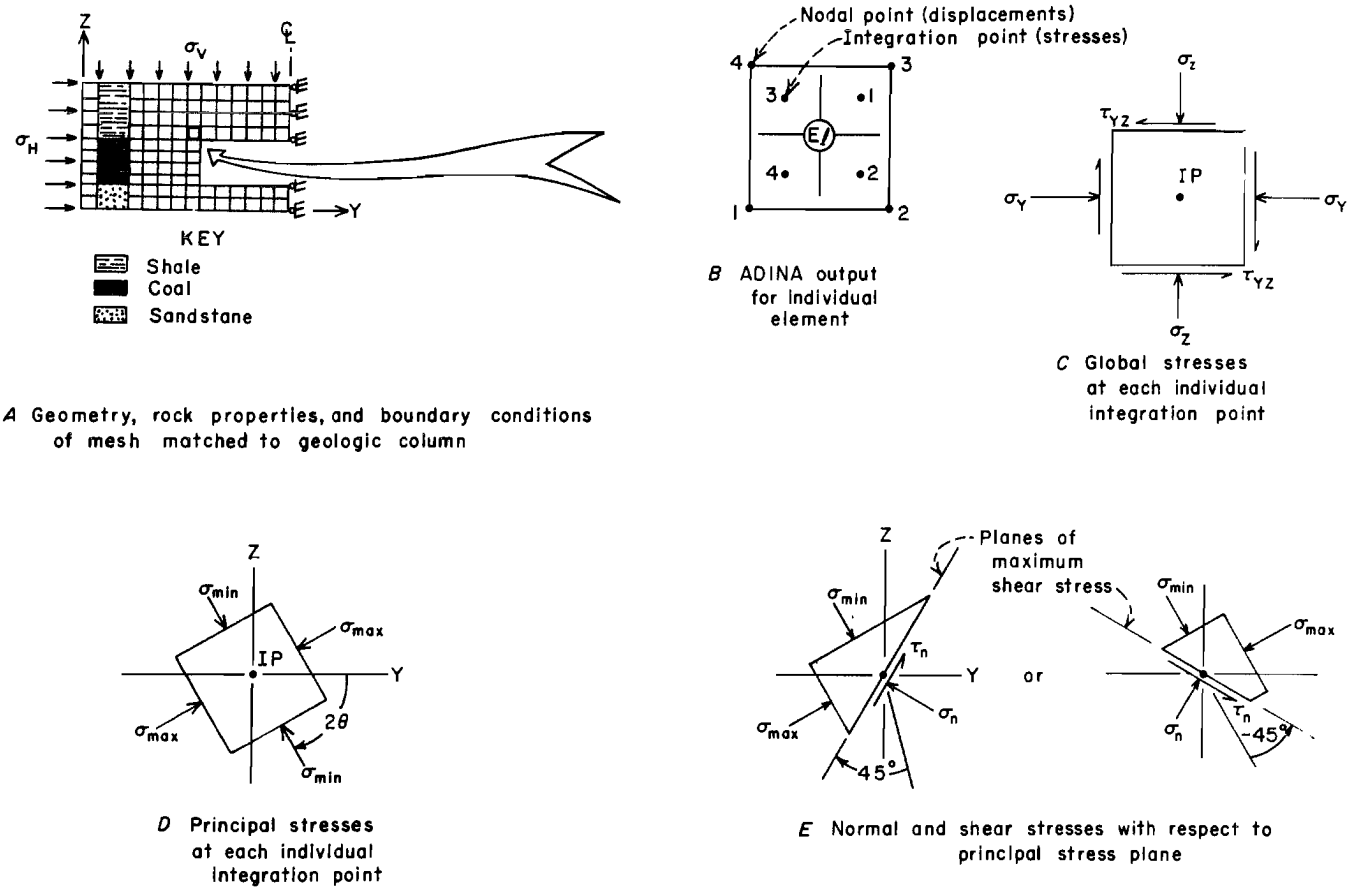

A Geometry, rock properties, and boundary conditions of mesh matched to geologic column

B ADINA output for individual element

C Global stresses at each individual integration point

D Principal stresses at each individual integration point

E Normal and shear stresses with respect to principal stress plane

FIGURE 3.–Stress output from finite-element analysis.

CRITERIA FOR ELEMENT FAILURE STRESS

Failure can occur in three ways--as a result of tension, compression, or shear. A brief review of commonly accepted failure criteria is given. Figure 4 summarizes the conventional failure envelopes determined from triaxial testing. Figure 4*B* represents the shear strength τ_F as a function of the cohesion S_o and the normal stress σ_n by the relationship

$$\tau_F = S_o + \sigma_n \tan \phi, \qquad (3)$$

where ϕ is the angle of internal friction developed from a family of Mohr's circle plots. Figure 4*C* expresses the compressive strength σ_F in terms of the uniaxial compressive strength C_o and the confining pressure σ_{min} by the relationship (12, 31)

$$\sigma_F = C_o + \sigma_{min} \tan\beta, \qquad (4)$$

where β is a constant that is related to the angle of internal friction by the relationship

$$\tan\beta = (1 + \sin\phi)/(1 - \sin\phi). \qquad (5)$$

The relationship of the failure stress and applied stresses is expressed (22, 32) in the form of an element safety factor:

$$SF = \sigma_F/\sigma_{max}, \qquad (6)$$

where SF is the element safety factor, and σ_{max} is the largest compressive principal stress acting on the element, as shown in figure 4. Therefore, if SF < 1, the element stress equals or exceeds the failure stress and element yielding occurs.

Element failure, for the purpose of this procedure, occurs at the level of the integration point of an element

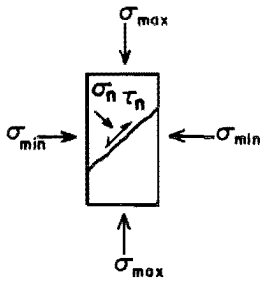

A Principal stresses applied to a triaxial compressive test

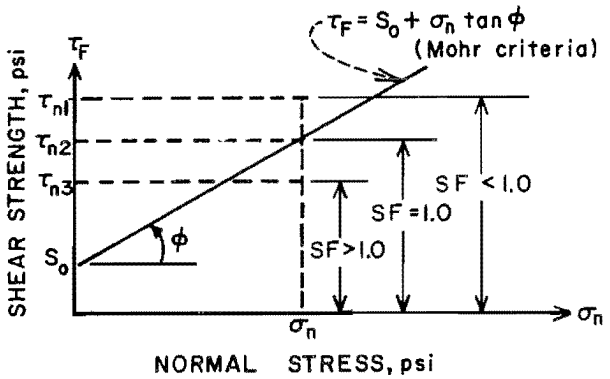

B Safety factor expressed in terms of shear and normal stresses

$$SF_{(Shear)} = \frac{\tau_F}{\tau_n} = \frac{S_o + \sigma_n \tan \phi}{\tau_n}$$

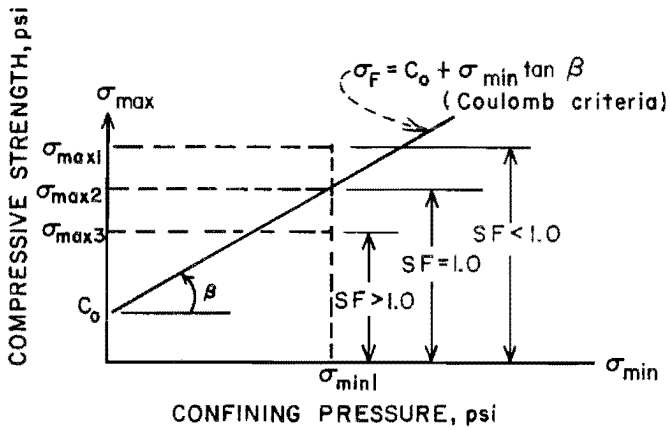

C Safety factor expressed in terms of principal stresses

$$SF_{(Comp)} = \frac{\sigma_F}{\sigma_{max}} = \frac{C_o + \sigma_{min} \tan \beta}{\sigma_{max}}$$

FIGURE 4.–Failure envelopes determined from triaxial testing.

(fig. 3*B*). If any integration point of an element fails because of compression and/or shear, then that element is said to have weakened. If failure occurs as a result of tension, then it is assumed that the safety factor for that integration point is zero. Thus, for integration point IP_I, the safety factor SF(i) meets the following criteria:

1. If IP_I is in compressive and/or shear failure,

$$SF(i) < 1.$$

2. If IP_I is in compression but has not failed,

$$SF(i) > 1.$$

3. If IP_I is in tension,[5]

$$SF(i) = 0.$$

The effective safety factor for the total element is found by averaging the safety factors of the individual integration points, or

[5]Criterion 3 is equivalent to an assumption that tensile strength is zero. In the work reported here, tensile stresses did not occur; therefore, criterion 3 was not operative. A more general criterion for tension, analogous to equation 6, would be of the form SF(i) = T/σ_T, where T = tensile strength and σ_T = applied tensile stress.

$$SF_{element} = \sum_{i=1}^{4} \frac{SF(i)}{4}. \quad (7)$$

At this point in the analysis, an assessment is made as to the degree of failure that has occurred throughout the structure. If no failure has been predicted to occur in any of the elements, the numerical portion of the analysis is complete. More than likely, though, some integration points in the coal rib will have failed. If the strength of the immediate roof and/or floor is low, it is possible that failure will be predicted here, too.

A computerized procedure was written to examine element failure in the areas of interest. The computer procedure is set up to survey every integration point in each element (if specified) for failure and automatically set up a new data input file, reducing the effective element strength and stiffness of the competent (unbroken) material by the safety factor, utilizing the following criteria at each iteration:

If $SF > 1.0$, then $E_{new} = E_{previous}$.

If $SF < 1.0$, then $E_{new} < SF_{element} \cdot E_{previous}$.

The concept of a yield factor (YF) formalizes the procedure of reducing the effective element strength and stiffness. The yield factor is defined as the ratio of the effective new Young's modulus, E_f, to the original Young's modulus, E_o:

$$YF = E_f/E_o. \quad (8)$$

YF is a number ranging from 0 to 1, where a YF value of 0 indicates total element disintegration, and a YF value of 1 indicates a fully intact material. Values of YF are used to define weakened material property sets in the following manner:

$$E_f = YF_f \cdot E_o, \quad (9)$$

$$\nu_f = 0.50 - YF_f \cdot (0.50 - \nu_o), \quad (10)$$

and

$$C_f = YF_f \cdot C_o, \quad (11)$$

where E_f and E_o are the effective and the original Young's moduli, ν_f and ν_o are the effective and the original Poisson's ratios, and C_f and C_o are the effective and the original uniaxial compressive strength. Equation 9 simply restates the definition of equation 8. Equations 10 and 11 are hypothetical and have not been tested by experiment.

For practical reasons, the iteration procedure is restricted to 22 material property sets. These are obtained from the 20 values of $YF = 0.05\eta$, for $\eta = 1$ to 20, plus the values $YF = 0.03$ and $YF = 0.01$. After each iteration, the following heuristic formulation determines the next YF for each element:

$$YF_{\tau+1} < SF_\tau \cdot YF_\tau, \quad (12)$$

where SF_τ is the element safety factor at iteration τ. Thus, if $SF_\tau < 1$, the element yield factor is decreased to the next lower yield factor below the product $SF_\tau \cdot YF_{\tau+1}$, unless it is already 0.01, in which case $YF_{\tau+1}$ remains 0.01.

This numerical procedure is justified by the fact that it has been shown (33) that progressive failure in rocks in compression is associated with a decrease in the elastic modulus. Fractured rock retains some degree of residual strength and elastic property because of the contact between the broken pieces and the internal friction forces produced by the existing confining pressures.

In developing any numerical procedure with the intent of simulating progressive pillar yielding and resulting stress redistribution, it is necessary to address the problem of solution convergence. At what point in the analysis should the solution be terminated? One must have a very definite impression and understanding of how the particular structure being analyzed behaves during the progressive failure process. Once a premise is assumed, it must be utilized consistently throughout the analysis.

There is a distinct difference between the physical instability that can occur in an actual mine structure and the numerical instability that might exist in any numerical scheme being used to represent the physical situation. The key to a successful solution lies in relating the numerical instability (generated by a computer) to the actual physical instability potentially existing in a mine structure. Each problem being solved by this method must be evaluated based on its own uniqueness. Although the conceptual approach to the problem may be the same, the convergence criteria for evaluating the potential for pillar and entry instability will be different from those for evaluating subsidence and caving-related problems. For example, in pillar yield problems, a consistent procedure may be repeated until a stage is reached where the new stress distribution, following some number of iterations, shows the stress at ribside reduced to a value equal to or very close to a predetermined engineering estimate of the uniaxial unconfined compressive strength of failed material at ribside. Once this point is reached within some practical degree of tolerance, the analysis is terminated and internal results are evaluated. Or as pictorially illustrated in figure 5, the analysis could be terminated when the load being transferred laterally and inward toward the pillar core as a result of the pillar rib yielding does not increase significantly. Simply stated, "engineering judgment" is required. It must be emphasized that the criteria selected for this report are examples only and that others could be used. In general, field measurements and observations provide the best guidelines and evidence for what criteria are appropriate.

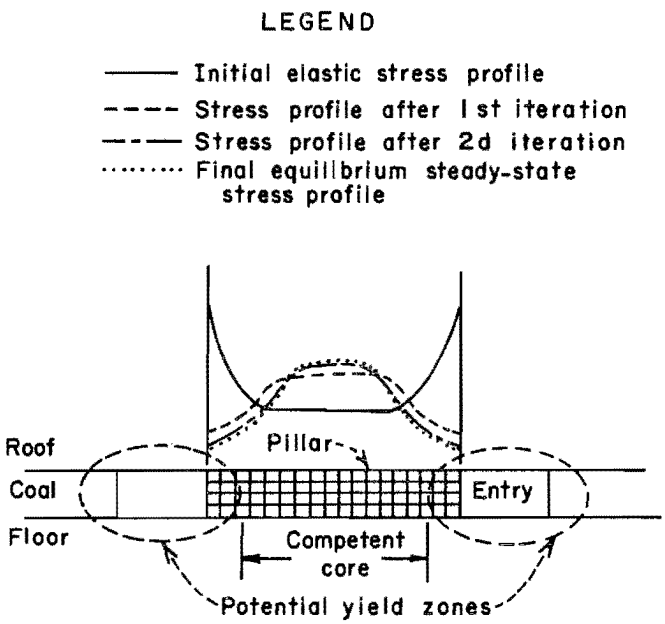

FIGURE 5.–Convergence criteria for overall pillar stability.

MODELING EFFECTIVE IN SITU MATERIAL PROPERTIES

How best to relate the material property inputs required for computer programs to the actual in situ material properties is still an area for research. In situ properties are often difficult to measure or to extrapolate from laboratory sample values, and considerations such as scale effects, jointedness, and possible localized material failure all complicate the problem. Measurement of nonlinear in situ material behavior in the postfailure region is especially difficult.

The computer programs used in the present approach, ADINA and MULSIM/BM, require input of effective linear-elastic material properties. The concept of an effective property refers to the equivalent of a homogeneous elastic isotropic body that would deform overall in the same effective manner as the actual rock mass. The following brief discussion indicates some of the considerations that entered into selection of these properties.

Effective In Situ Modulus

Two interrelated indices are especially good indicators of the condition of a rock mass. One is the rock mass rating, or RMR, as developed by Bieniawski (34-35); the other is the Norwegian Geotechnical Institute's tunneling quality index, or Q (36). These indices are also explained in detail by Hoek and Brown (37) and are related by the empirical equation (35, 37)

$$RMR = 9 \ln Q + 44. \quad (13)$$

The modulus of deformation is the ratio of stress to strain during loading of a rock mass, including both elastic and inelastic behavior. It is empirically related to these indices by the following equation (38):

$$E_m = 2\ (RMR) - 100, \qquad (14)$$

where E_m = modulus of deformation, in GPa. (1 GPa = 145,040 psi).

The modulus of deformation may be used as the basis of an effective in situ elastic modulus to be used for the computer analysis. In coal-bearing strata, the in situ rock mass is typically a layered and jointed medium whose properties are only remotely related to those of a small laboratory sample. When undermined, nonelastic effects such as the cracking open of joints occur as the rock mass deflects and settles upon a gob zone. Thus the modulus of deformation, or effective modulus, of such a rock mass may be relatively low. Therefore, an assumed value of E for coal equal to 400,000 psi, corresponding to a relatively low RMR, was used in the analyses reported here.

Effective In Situ Strength

A method of adjusting measured values of the uniaxial strength to account for size and shape effects has been given by Hardy (39-40) as cited by St. John (41, p. 30):

$$\sigma_R = \left[\frac{V_L}{V_c} \right]^{\alpha} \cdot \left[\frac{S_L}{S_c} \right]^{\beta} \cdot \sigma_L, \qquad (15)$$

where

σ_R = reduced strength, psi,

σ_L = laboratory strength, psi,

V_L = volume of laboratory rock sample, ft^3,

V_c = rock mass representative volume, ft^3,

S_L = height-to-width ratio of laboratory sample,

S_c = height-to-width ratio of rock mass representative volume,

β = shape effect factor,

and

α = volume reduction factor,

= 0.05 for excellent rock $Q > 100$

= 0.10 for $10 < Q < 100$

= 0.15 for $Q < 10$,

where Q is the rock mass tunneling quality index.

The original work by Hardy leading to this equation was based on a study of the behavior of coal pillars and identified values of $\alpha = 0.118$ and $\beta = 0.833$ (39), as cited in St. John (41).

This equation was used in the present work to identify the lower limit for a range of compressive strength values for a coal pillar. A volume reduction factor of 0.15, corresponding to a weak material, was considered appropriate for coal. The resulting compressive strength range considered in the analyses was from the full strength of a laboratory sample down to one-tenth of that value.

Effective In Situ Gob Modulus (25)

A theoretical mathematical model of gob zone behavior was first developed by Salamon (42). Mozumdar (43) demonstrated the application of this theoretical model in mine structural analysis using the finite-element method.

The Salamon model of gob behavior is that of a rubbled mass, formed by caving of the immediate roof layers overlying an excavation, that bears no load until it is compacted by the weight of the main, uncaved rock mass. The load-bearing capacity of the gob increases with compaction, in this mathematical

representation, toward an asymptotic limit that represents the volume of the original uncaved rock. The resulting stress-strain relationship is given by Mozumdar (43) as follows:

$$p = k'w/(m - w), \qquad (16)$$

where

p = gob resistance, psi,

k' = a material constant, psi,

m = extracted seam height, ft,

and

w = amount of gob zone roof-to-floor convergence, ft.

To convert equation 16 into a form using stresses and strains, substitute σ_{NL} for p, and divide both the numerator and the denominator by the gob height, g, resulting in the following equation:

$$\sigma_{NL} = k'\varepsilon_g/(\varepsilon_{max} - \varepsilon_g). \qquad (17)$$

Salamon (42) gave a value of 133 psi for the constant k' as a representative value for European coal measure rocks.

Finite-element analyses conducted by the Bureau using this equation to represent gob behavior have shown that structural analysis using this theory can give useful results for gob behavior. However, the value of k' given by Salamon is thought to be too low for western U.S. conditions, and recent Bureau analysis has pointed to a higher value, in the neighborhood of 1,700 psi, consistent with a linear, secant in situ gob modulus of 20,000 psi (25, 28).

MULSIM/BM uses a linear approximation to the nonlinear curve of equation 17. This linear approximation corresponds to use of a secant elastic (Young's) modulus of the in situ stress-strain response of a gob zone, as shown in figure 6. The linear approximation was chosen to simplify program execution with resulting savings in execution time and also in computer core storage requirements.

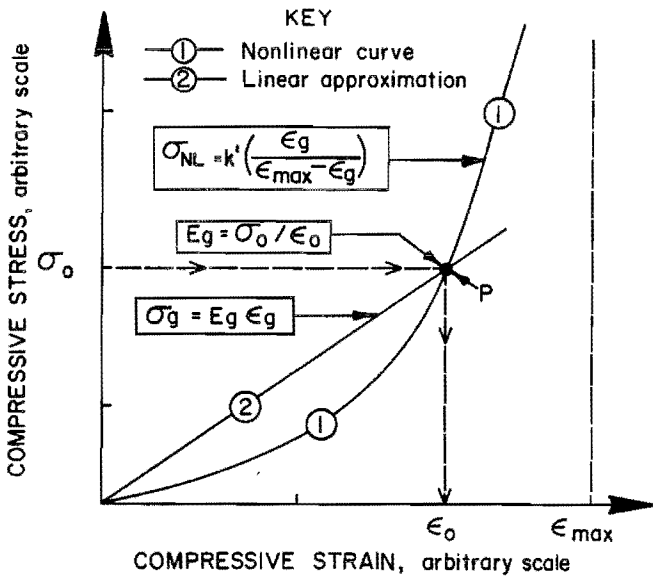

FIGURE 6.–Selection of a secant elastic modulus for gob.

Figure 6 (25) shows the recommended method of selecting a secant in situ gob modulus to correspond to the Salamon curve as applied to a particular virgin overburden stress level. In figure 6, σ_o is the virgin overburden stress level and ε_{max} is the amount of compressive strain that would correspond to a gob-zone convergence equal to the extracted seam height, m. ε_o is the strain corresponding to an amount of gob convergence, c, that just enables the gob to sustain the overburden stress σ_o. The resulting secant in situ gob modulus, E_g, is then given by

$$E_g = \sigma_o/\varepsilon_o. \qquad (18)$$

The MULSIM/BM user inputs an adjusted gob modulus, E_{GM}, that is related to the secant in situ gob modulus by the following equation:

$$E_{GM} = E_g(m/g), \qquad (19)$$

where

m = seam height,

and

g = assumed or measured in situ gob zone height.

The reason for this final adjustment is explained in Bureau IC 9168 (25) and a related paper (28) and also in the "Model Characteristics" section of the present report. Briefly, MULSIM/BM does not distinguish between the gob zone height and the original seam height, because the underlying elastic theory assumes that these heights are negligible compared with the dimensions of the rock mass. The purpose of providing the adjusted gob modulus, E_{GM}, is to enable the program to calculate correct closure values for the gob zone.

In the implementation of this linear gob model in MULSIM/BM, the program begins with a working assumption that all elements of the grid are initially at equilibrium with the virgin overburden stress field. While for an original seam material (coal) this working assumption corresponds to a condition of zero roof-to-floor closure across the seam, for a gob zone it corresponds to an initial closure, c, equal to the product of ε_o multiplied by the gob zone height, g. This initial working assumption is normally considerably different from the final solution for a particular mining situation.

In the process of iteratively solving for a balanced set of closures, the program normally ends up reducing the closures of gob elements, thus reducing the calculated stress carried by those elements, and increasing the closures of coal elements near the gob zones, thus increasing the stress carried by those elements. In the coal elements, this process results in calculation of stress abutments. In the gob, this process results in calculation of stress-relieved areas near adjacent unmined coal pillars or blocks.

In calculating the precise stresses carried by the gob, the program uses the secant modulus, and in the destressed gob regions the stresses calculated by the secant modulus are slightly higher than the stresses that would be calculated by use of the nonlinear equation 17. The total stress levels calculated by either method are, however, sufficiently low compared with the overburden stresses that the resulting disparity should in most cases have little impact on the stresses calculated for other areas of an analysis.

Recent Bureau analyses have used the MULSIM/BM gob material model successfully to analyze the stress transfers around longwall panel gob zones (28, 44). These analyses have used an assumed in situ elastic gob modulus of 20,000 psi, a number that lies within the middle of a range of 1,000 to 47,000 psi reported by Peng (45, p. 222) for rubbled rock material or gob.

DEMONSTRATION OF MINE DESIGN PROCEDURE

Historically, ground control problems in longwall panel entries have been most severe in the tailgate area because of concentrated abutment pressures, as illustrated in figure 7. These problems are magnified when mining over or under old workings. Many current longwall mining operations in the United States have experienced severe localized ground control conditions as a result of interaction between two or more mining operations, one above the other. These problems will continue to grow in importance as operators are forced to open new seams above or below seams currently being mined.

THE IN SITU SITUATION

Using the procedure described above, a rock mechanics structural analysis was performed of a typical situation encountered when mining under old workings. Figure 8 shows an overlay of two mine plans of Utah Power and Light Co.'s Deer Creek and Wilberg Mines near Orangeville, UT. The upper seam represents old room-and-pillar workings in the Deer Creek Mine. The lower seam represents portions of three adjacent successive longwall panels in the Wilberg Mine, separated by the two-entry gateroad systems. The situation is analyzed here as it existed

during the period 1983-84. Unmined pillars in the Deer Creek Mine transfer load concentrations onto the underlying Wilberg Mine, located under 68 ft of interburden. Given this situation, the problems are (1) to determine the induced loading history for the chain pillar system that separates adjacent longwall panels, (2) to predict the degree and extent of progressive failure of a pillar, from initial entry development through retreat mining of adjacent panels, and (3) to account for the effects of multiple-seam interaction.

The chain pillar is loaded in situ by two major mechanisms: the redistribution of overburden load caused by the remnant mine structures in the overlying seam and load transfer caused by mining of the

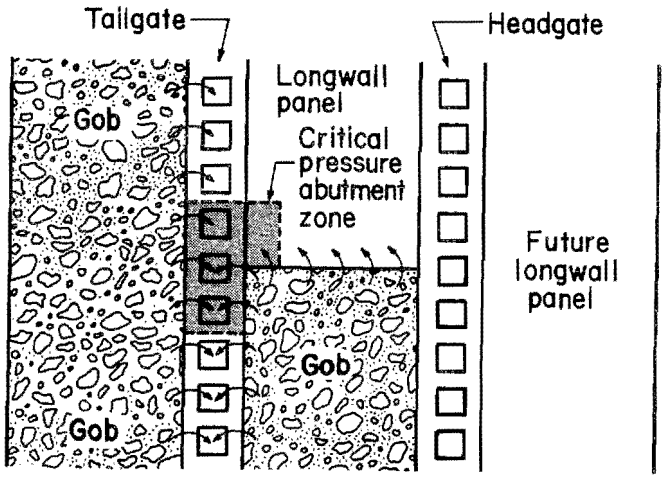

FIGURE 7.–Critical pressure abutment zone in tailgate entry.

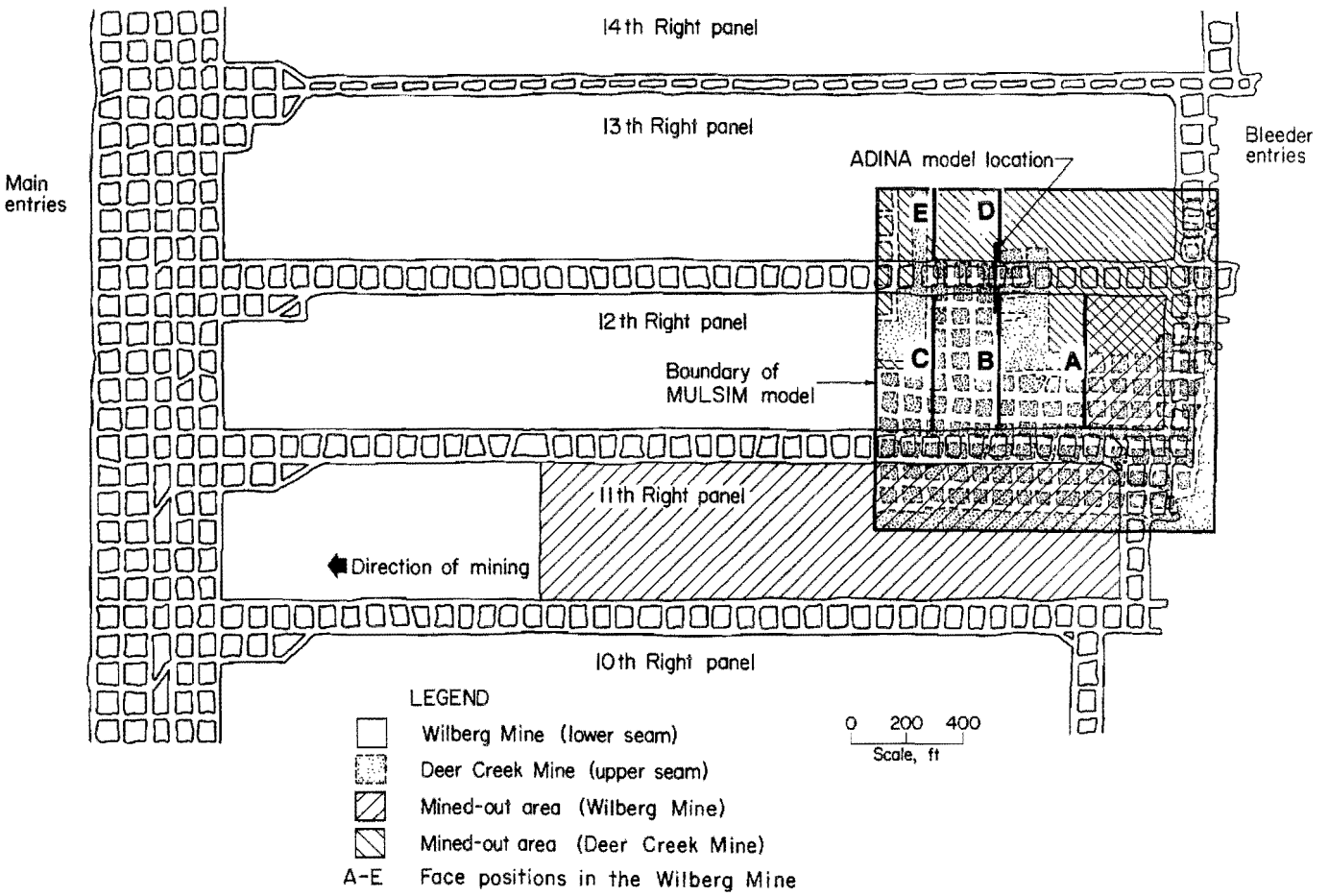

FIGURE 8.–Plan view of Wilberg Mine, situated under Deer Creek Mine.

adjacent longwall panels. The mining system in the upper seam does not change; therefore, the loading distribution from the upper seam remains constant or almost constant. In contrast, load transfer caused by mining of the adjacent panels varies greatly, depending on the face location. Both mechanisms continuously superimpose their loads on the chain pillar being studied. The minor effects of artificial support, such as cribs, in the entries were not included.

MODELING THE IN SITU SITUATION

To study the multiple-seam interaction problem, MULSIM models were generated for face positions A through E, shown in figure 8, to obtain stresses and displacements at the two coal seam levels. Face positions A, B, and C in the 12th Right longwall panel are located at respective distances of 300 ft inby, 10 ft inby, and 200 ft outby the location of the ADINA model. Face positions D and E in the 13th Right longwall panel are located at respective distances of 10 ft inby and 200 ft outby the location of the ADINA model.

Figure 9 illustrates the modeled geometry of structures in the two seams located within the bounds of the MULSIM model. A portion of the MULSIM element grid is shown superimposed in figure 9 to indicate the level of detail. Figure 10 shows the details of the ADINA model designed to study a vertical cross section of the 82-ft wide chain pillar separating the 12th Right and 13th Right panels located between crosscuts 36 and 37. Only the portion of the mesh in the area of interest is shown.

MODEL CHARACTERISTICS

The five MULSIM models each consisted of 144 blocks per seam, arranged in a 12 by 12 grid; each block contained 25 elements, as shown previously in figure 9.

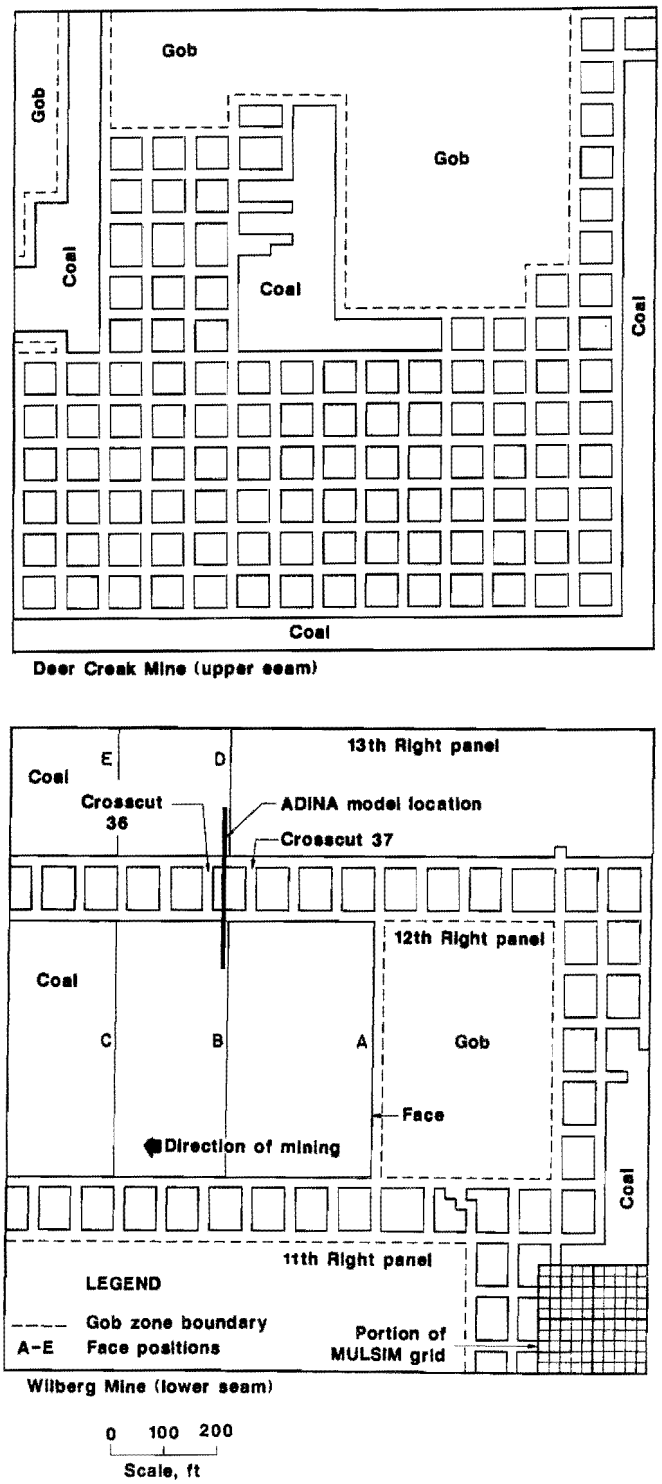

FIGURE 9.–MULSIM model as defined for face positions A and B.

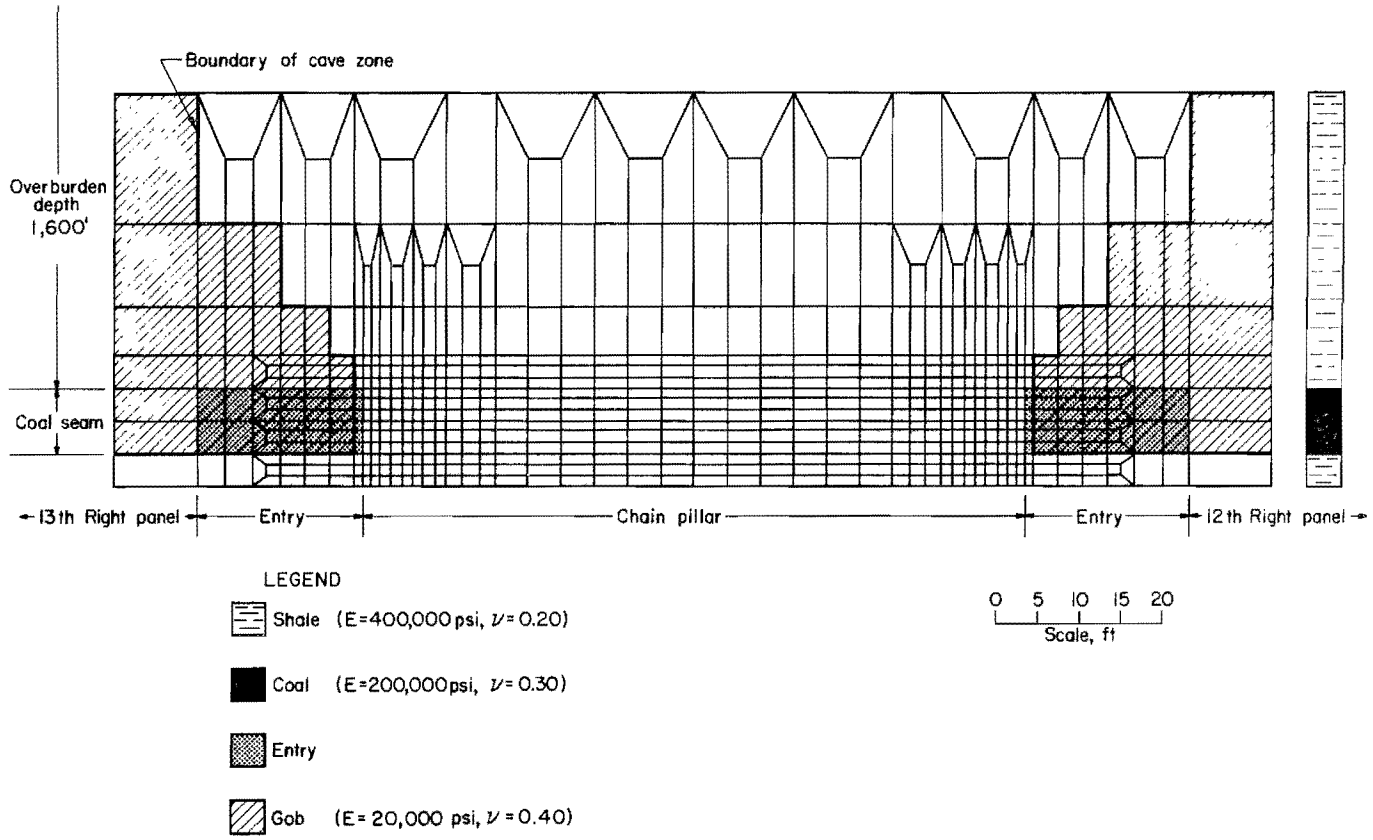

FIGURE 10.–Portion of ADINA model showing chain pillar and entries.

MULSIM assumes a uniform element size. For this analysis, each element represented a 20- by 20-ft area, and the total MULSIM grid represented a 1,200- by 1,200-ft area of each seam. The total area modeled was moved slightly for different face positions to maintain the modeled face positions near the center of the grids. The seam thickness modeled within each seam was 8.0 ft. The elastic properties, shown in table 1, used in the MULSIM models were based on engineering estimates influenced by the considerations discussed previously in the section "Modeling Effective In Situ Material Properties." The full laboratory compressive strength of coal was used in the initial analyses; later refinement involved investigating a reduced strength range. The assumed stress field was a vertical compressive stress of 1.1 psi/ft of depth and horizontal compressive stresses of 0.5 times the vertical stress. The lower seam was under 1,600 ft of overburden, and the upper seam was under 1,524 ft of cover. The modified MULSIM solution algorithm assumes that coal elements are at equilibrium with the overburden stress at the nominal seam thickness and that gob elements support no load until they are compressed. In this way, the MULSIM solutions normally indicate a considerable load transfer away from the gob zones and openings and onto the intact coal.

The ADINA model representing face positions A and B used 1,034 node points to define 1,010 two-dimensional plane-strain

TABLE 1. - MULSIM model elastic properties

Material	Young's modulus (E_o), psi	Poisson's ratio (ν_o)
Rock mass...	400,000	0.20
Intact coal.	200,000	.30
In situ gob.	20,000	.40
Gob (MULSIM)	5,000	.40
Gob (ADINA).	20,000	.40

quadrilateral elements. The boundary conditions consisted of prescribed horizontal and vertical displacements for each boundary node compatible with the appropriate MULSIM results. For face positions C, D, and E, the modeling details changed slightly because the element "birth-death" option was used to simulate excavation and gobbing. In addition, limitations in the ADINA prescribed-displacement option required use of concentrated forces, applied through a vertical and a horizontal stiff truss element at each boundary node, to specify the appropriate boundary node displacements.

In order to simulate the same gob stiffness and still maintain compatibility between the displacement-discontinuity MULSIM models and finite-element ADINA models, an adjusted gob modulus is used, as mentioned previously. Figure 11 illustrates the concept using a simple spring analogy. Program MULSIM requires that all elements in the grid for a particular seam to have the height of the original seam thickness. In reality, of course, the height of a gob zone is higher, typically about three to four times the seam height, depending on the bulking factor of the immediate roof, which caves to fill the excavation. The height of the gob zone in the ADINA model was more realistically modeled as being four times the height modeled with the MULSIM model, as shown in figure 10. For the MULSIM model, from figure 11, the gob stiffness can be expressed as

$$K_{GM} = \frac{F}{\delta} = \frac{AE_{GM}}{m}, \qquad (20)$$

and for the ADINA model, the gob stiffness can be expressed as

$$K_{GA} = \frac{F}{\delta} = \frac{AE_{GA}}{4m}. \qquad (21)$$

In order to simulate the same gob stiffness in both models, let

$$K_{GM} = K_{GA}.$$

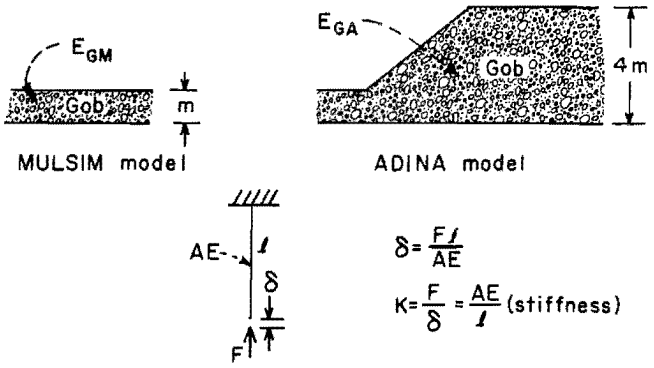

FIGURE 11.–Equivalence of gob stiffness between MULSIM and ADINA models.

Therefore,

$$\frac{AE_{GM}}{m} = \frac{AE_{GA}}{4m}, \qquad (22)$$

and

$$4E_{GM} = E_{GA}. \qquad (23)$$

Therefore, the Young's modulus value for the ADINA gob represents the assumed in situ gob secant modulus, E_g, and is four times the adjusted value used in the MULSIM model. The ADINA "birth-death" option was used to represent excavation of coal and the change from rock or coal properties to gob properties in two distinct steps for each model run. This ADINA process, like the MULSIM solution, did not allow gob elements to sustain load until they were additionally compressed by the postexcavation load transfer.

For this example, to demonstrate the process simply, the number of iterations was limited to five for each face position. This cutoff allowed sufficient iterations to effect most of the large changes in element strength but did not achieve final equilibrium for all elements. Since a pillar element was never allowed to become stronger than its final strength for the previous face location, the effect of the five face positions on element strengths was cumulative.

RESULTS OF MODELING ANALYSIS

This section presents model analysis results for the five face positions designated in figure 8. Displacement-discontinuity results are presented in the form of three-dimensional stress plots, figures 12 and 13. Finite-element results are presented in two dimensions, figures 14 and 15. Gradual pillar rib deterioration and the change in stress distribution predicted to occur through a vertical cross section of the typical chain pillar are presented for each face position. The effects of seam interaction are noted.

Figures 12 and 13 illustrate the influence of old workings in the upper Deer Creek Mine on the vertical stress distribution in the lower Wilberg Mine for face position A. The gob zone in the overlying Deer Creek Mine transfers load laterally to the barrier pillar, which channels the stress down to the Wilberg chain pillars. Figure 12*B* shows this resulting additional stress concentration ahead of the face on the gateroad system separating the 12th Right and 13th Right longwall panels. In comparison, stress concentrations in the absence of seam interaction are depicted in figure 13.

Figures 14 and 15 illustrate the progressive pillar rib deterioration predicted to occur in the chain pillar. Table 2 lists the peak stress magnitudes and extents of yielding for the face positions A through E. The load distribution from the upper seam has a significant influence on the pillar. The degree and extent of yielding vary from one side of the pillar to the other. Initially, for face position A, more yielding occurs on the 13th Right panel side of the chain pillar because of the influence of the remnant pillar in the upper seam that supports load from the upper seam gob zone. As the 12th Right panel

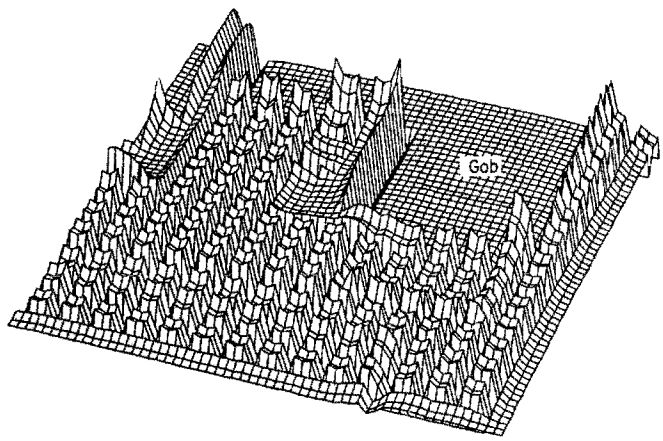

A Deer Creek Mine (upper seam)

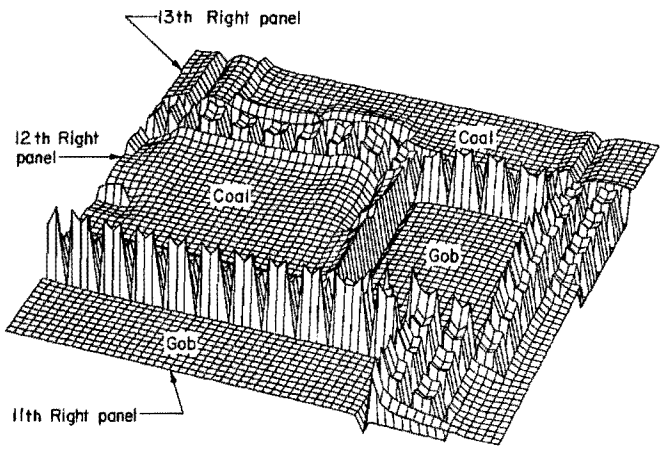

B Wilberg Mine (lower seam)

FIGURE 12.–Three-dimensional vertical stress plot from MULSIM face position A.

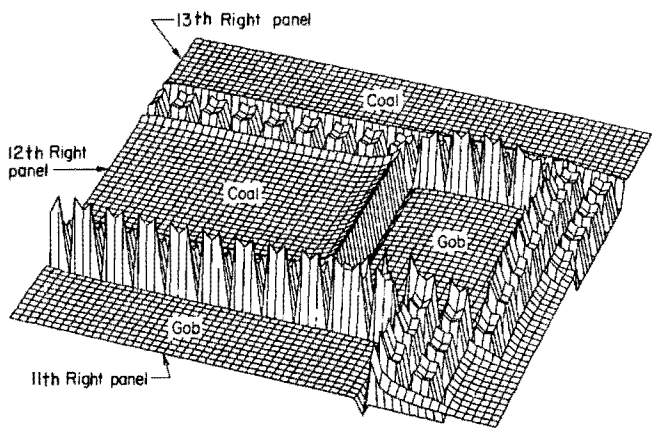

Wilberg Mine

FIGURE 13.–Vertical stress plot for face position A without upper seam mining.

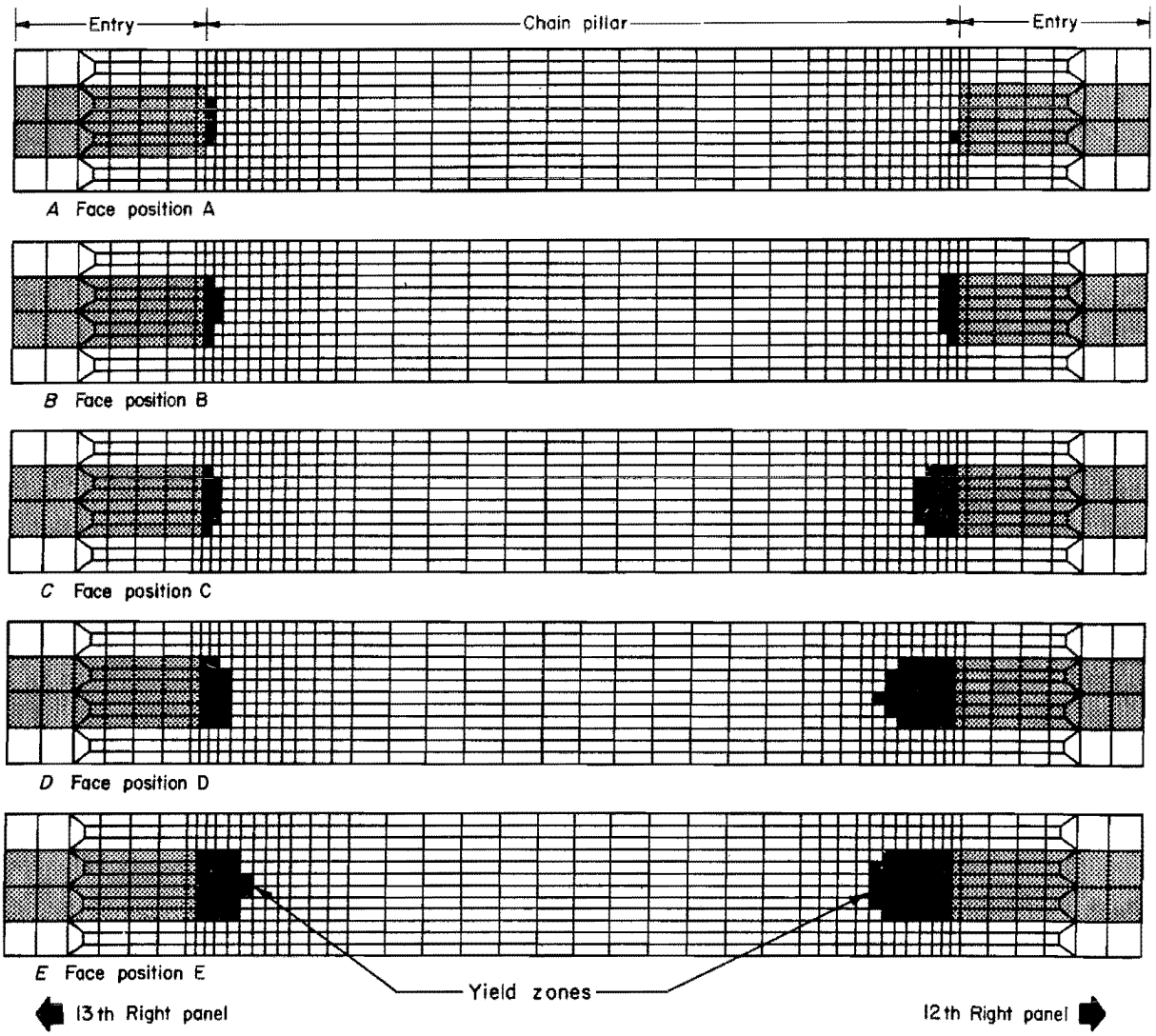

F Final computed yield factors in coal pillar for face position E

FIGURE 14.–Progressive pillar rib failure as a function of face position (compressive strength = 4,000 psi).

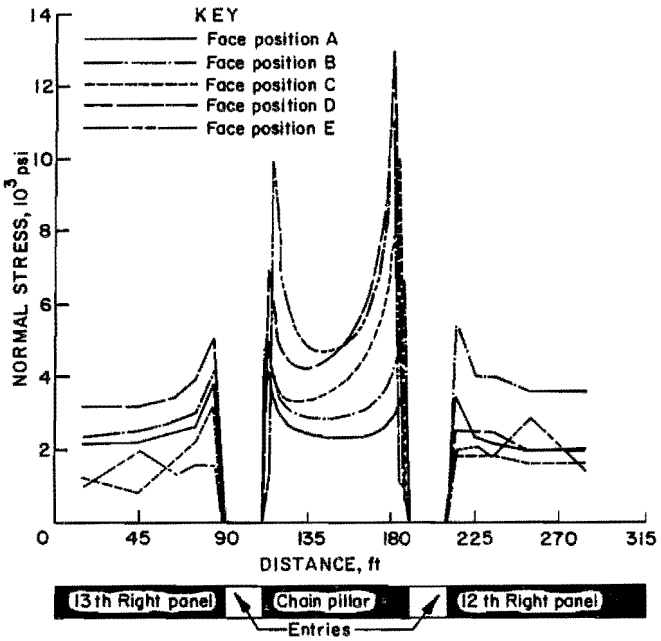

FIGURE 15.–Change in normal stress profile through pillar cross section for face positions A through E from numerical modeling analysis (compressive strength = 4,000 psi).

face advances to position B, the abutment pressures from the mined-out 12th Right panel begin to predominate, cause more yielding (fig. 14*B*), and produce a higher peak stress (fig. 15) on the 12th Right panel side of the chain pillar. Additional yielding on the 12th Right panel side of the chain pillar occurs for face position C. As the 13th Right panel is mined, the degree and extent of pillar rib failure continues to increase, as illustrated in figures 14*D* and 14*E* for face positions D and E, respectively. Figure 14*F* shows the final computed yield factors after both panels have been mined. The maximum partial failure extends almost 9 ft into the pillar rib.

Figure 15 summarizes the modeled changes in normal stress across a section of the chain pillar, through a line at the middle portion of the pillar, as the adjacent panels are mined and the pillar ribs yield. These stress changes accompany the progressive failure in the pillar for face positions A through E. Face position A shows an initial pillar core stress of approximately 2,200 psi. The pillar core stress increases to almost 3,000 psi for face position B, and the peak abutment stress shifts from the 13th Right panel side to the 12th Right panel side. For face position C, the load transfer is more evident as the pillar core stress increases to an average value of approximately 4,000 psi and the peak stress shifts inward toward the middle of the pillar. The gob carries a normal stress of 1,100 psi, approximately one-half the original overburden pressure. Both the average pillar core stress and the peak pillar stress continue to increase for face position D. Face position E shows the highest overall pillar core stress, approximately 5,000 psi. The average pillar core stress in the chain pillar increased approximately 127 pct, and the peak pillar abutment stresses increased approximately 242 pct for the change in loading conditions from face position A through face position E in the numerical models.

TABLE 2. - Peak stress magnitude and distance into pillar rib as a function of face position (compressive strength = 4,000 psi)[1]

Face position	Left-side peak stress		Right-side peak stress	
	Magnitude, psi	Distance from left rib, ft	Magnitude, psi	Distance from right rib, ft
A.....	4,350	1.50	3,717	1.50
B.....	4,981	2.67	6,694	2.67
C.....	5,072	2.67	10,104	5.33
D.....	6,958	4.00	12,994	8.00
E.....	9,949	5.33	11,363	9.33

[1]See figure 15.

COMPARISON OF MODELING RESULTS WITH ON-SITE DATA

To verify the numerical results, a field study was initiated in February 1984 at the Wilberg Mine. Eleven holes were drilled to depths of 20 ft into the chain pillar for installation of vertical and horizontal borehole pressure cells (VBPC's and HBPC's) and cylindrical pressure cells (CPC's) connected to continuous recording devices. The instrumentation plan is shown in figures 16 and 17*B*.

Pressure changes were continuously monitored and recorded during retreat mining of the 12th Right and 13th Right longwall panels. Using a theoretical method developed by the Bureau (46-47), vertical stresses at each hole were estimated from each set of cell pressures. Figure 17*A* presents the vertical stress profiles across the chain pillar corresponding to the four face positions, A through D, shown in figure 8 for the model analysis, plus one intermediate position, I. Data corresponding to face position E were not available because the recorder station became inaccessible when the 13th Right longwall was mined past the recorder location. Figure 18 illustrates the continuous vertical stress history in the chain pillar, measured in six of the boreholes through the complete mining of the 12th Right and 13th Right panels. The other boreholes were omitted for clarity.

Although the field data are neither complete nor conclusive, the field results can be compared with the numerical modeling results. The comparison should be considered more on a qualitative than a quantitative basis because determining accurate absolute stresses from BPC pressures is still a major area of study. Additional methods for

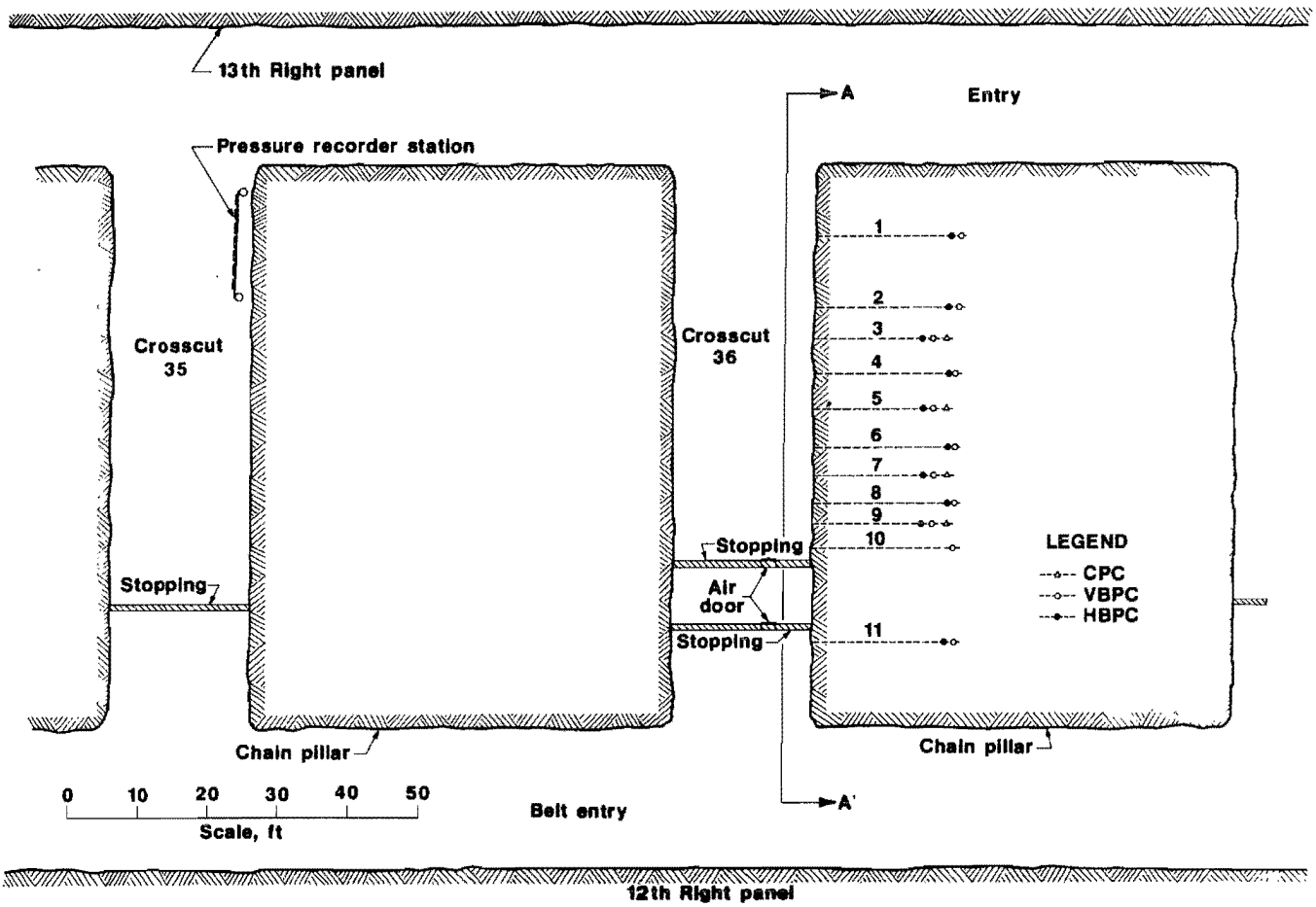

FIGURE 16.–Chain pillar instrumentation plan.

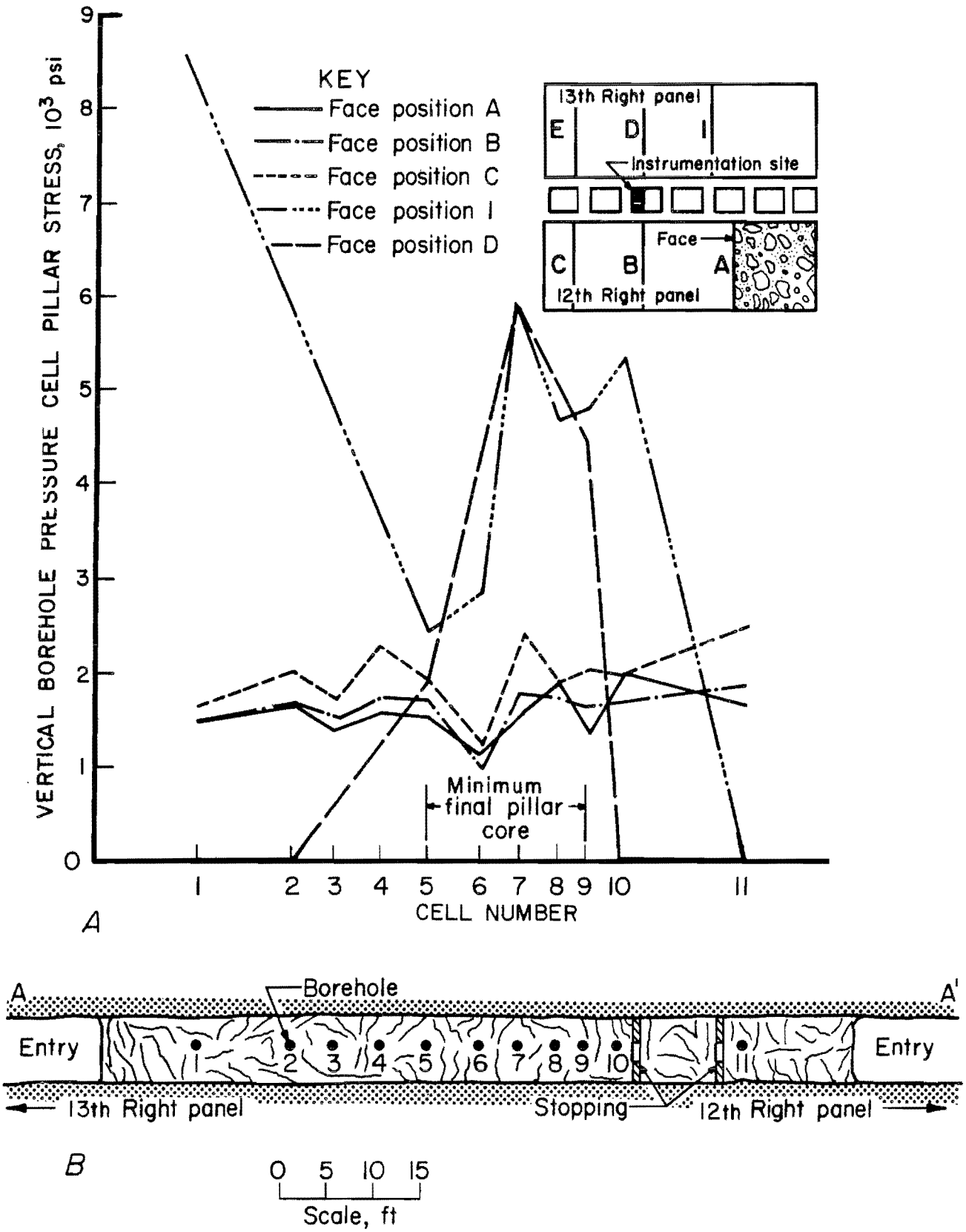

FIGURE 17.–Normal stress profiles through pillar cross section from field data. *A*, Vertical borehole pressure cell pillar stress value versus face position; *B*, elevation view of chain pillar instrumentation plan (view A-A', figure 16).

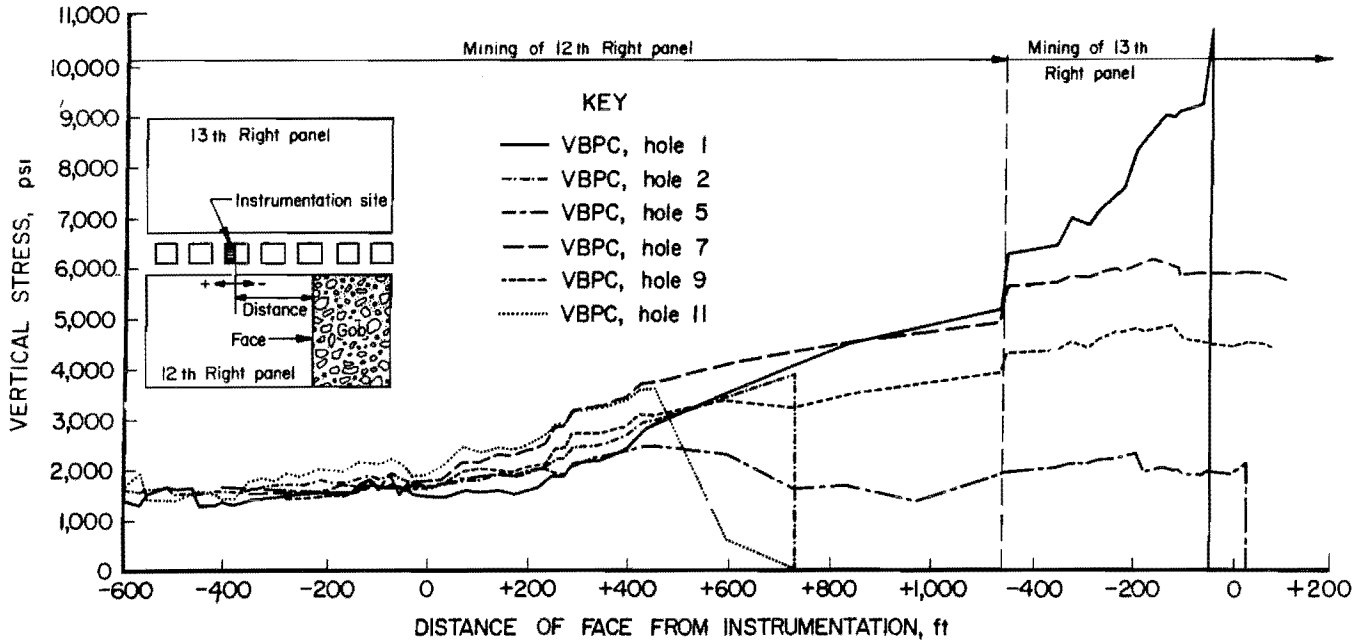

FIGURE 18.–Vertical borehole pressure cell stress in chain pillar as a function of face distance.

determining stress are available, and one such method was recently developed by the Bureau (48). This method uses a logarithmic relationship between cell pressure change and rock stress change. The method also depends on the setting pressure and the cross-sensitivity of the gauge to transverse loading. More important than which method is the most accurate, however, are the following: a measure of the extent of yielding into the pillar, the location of stress buildup, and the timing of stress changes and yielding relative to face position.

Figure 18 shows that vertical stress changes increased only slightly and were uniform throughout the pillar until the 12th Right panel face advanced to the instrumentation site. After the panel face passed the instrumentation site, the stresses began to increase rapidly. When the panel face reached approximately 400 ft outby the instruments, the reading of stress change in hole 11 began to decline, reaching zero when the face was 750 ft outby the instruments. This decline is consistent with a gradually yielding pillar rib.

During mining of the 13th Right panel, hole 1, nearest the active panel, began to receive additional stress rapidly as the load was apparently transferred from the panel to the pillar. The peak stress at hole 1 reached a maximum of seven times its initial setting pressure when the face was approximately 50 ft inby the instruments, and then the pressure in the cell suddenly dropped to zero. This sudden loss of stress suggests either a sudden, complete failure of that portion of the pillar rib, or instrument failure.

As the 13th Right panel passed position D, only the pressure cells located in holes 5, 7, and 9 still indicated vertical pressure readings. The pressure cells in holes 2 through 4 had lost pressure by that time, because either the equipment have failed or the coal in the area of the cells had become fractured. This face position indicates possible pillar rib yielding, leaving a narrow central core. The zone including holes 5, 7, and 9 was within the remaining solid pillar core, as noted in figure 17*A*. This narrow core is the minimum width that the remaining core could be. If any cells failed, as opposed to coal yielding, the core could be larger than indicated. Shortly after the panel passed position D, as observed in figure 18, the vertical pressure cell reading in hole 5 dropped to zero. In this case

no preceding stress increase occurred, therefore, the pressure drop was attributed to local fracturing rather than to pillar or cell failure.

In comparing the field data from figure 17*A* with computer modeling data in figure 15, a gradual increase in vertical stress in the pillar core is shown as mining advances. A slightly higher peak stress occurred on the 12th Right panel side as that panel was mined. To facilitate comparison, a stress profile was included in figure 17*A* for an intermediate position (I) of the 13th Right panel face 195 ft inby the cells. This profile shows a peak stress of 5.5 times its setting pressure at hole 1. No field data were available after face position C for holes 2 through 4; however, hole 1 was holding pressure so it was assumed that the coal between holes 1 and 5 was still intact. Therefore, a line was drawn in figure 17*A* from the data point for hole 5 to the data point for hole 1. These results compare reasonably well with the modeling results in figure 15, even though this particular face position was not modeled.

These findings agree qualitatively with the numerical modeling analysis presented in figures 14 and 15. The peak stresses measured with the BPC's along the pillar ribs are not, however, as high as the model predicts. One reason for this difference may be that no borehole pressure cells were installed within 10 ft of the pillar rib for stress measurements, while the peak modeled stresses for face positions A through C occurred at only 2 to 5 ft from the rib. A second reason is that the model assumes a linear-elastic, isotropic material. The model material acts as a continuum and does not simulate fractures, which act in situ to reduce confinement and strength. To some extent, the artificial confinement created around the pillar by the elastic model causes unrealistically high stresses near the pillar edge. A third and most important reason involves the yield criteria assumed in the model analysis. The uniaxial compressive strength used, 4,000 psi, is a typical laboratory value for Wilberg coal, but if a lower value that correlated more closely to in situ strength had been used, the extent of yielding in the pillar would have been proportionately greater. Regardless of the quantitative differences, the field studies and initial numerical modeling studies agreed upon the general trends of increasing pillar core stress and rib yielding.

REFINEMENT OF NUMERICAL MODEL ANALYSIS

Additional model analyses were performed using the above described procedure to more closely match the prediction values with the field measurements. As was previously mentioned, it was not possible to compare directly the model and field results at face position E, as shown in figure 9, because the recorder station, shown in figure 16, became inaccessible after the longwall face of the 13th Right panel passed outby.

EFFECTS OF UNIAXIAL COMPRESSIVE STRENGTH

Initial predictions indicated that the width of final pillar core was approximately 67 ft (at face position D), whereas the field measurements suggest the remaining pillar core width to be approximately 40 ft (at face position D). The quantitative discrepancies can be attributed to the choice of material property values. The value used in the initial model analysis was a laboratory value for the uniaxial compressive strength of coal and did not represent true in situ behavior. Results from using two lower values of uniaxial compressive strength were evaluated to determine the sensitivity of this parameter on the extent and degree of pillar rib yielding. Since the effective in situ compressive strength of the Wilberg coal was lower than the laboratory value, model results using these two lower values resulted in greater predicted yielding. The first value, 1,480 psi, was obtained by an application of the reduction formula by Hardy (39-40) as cited by St. John (41), discussed previously in the section "Modeling Effective In Situ Material Properties." The second

value, 400 psi, assumed the in situ uniaxial compressive strength value to be 10 pct of the laboratory value, a reduction thought to represent the lower limit of the range for in situ values.

Figures 19 and 20 illustrate the results from the numerical modeling analysis using a uniaxial compressive strength value of 1,480 psi. Table 3 lists the peak magnitudes and extents of yielding for the five face positions modeled. These results show that the overall degree and extent of pillar rib yielding increases, and the position of peak abutment stress shifts inward into the pillar core when compared with the results shown in figures 14 and 15 based on a uniaxial compressive strength of 4,000 psi. The overall stress level in the pillar core remains relatively the same; however, the peak abutment stresses into the pillar ribs decrease. The width of pillar core at face position D is 58 ft, as shown in figure 19, compared with 40 ft estimated from field measurements.

Figures 21 and 22 illustrate the results from the numerical modeling analysis using a uniaxial compressive strength value of 400 psi. Table 4 lists the peak stress magnitudes and extents of yielding for the five face positions modeled. These results also show that as the value of uniaxial compressive strength further decreases, the overall degree and extent of pillar rib yielding again increases, and the position of peak abutment stress continues to shift inward into the pillar core. The predicted width of final pillar core is shown in figure 21*E*. As noted previously, the overall stress level in the pillar core remains relatively the same as for the higher values of uniaxial compressive strength, but the peak abutment stresses into the pillar ribs continue to decrease, reflecting the softer material. The width of pillar core at face position D is 46 ft, compared to 40 ft obtained from field measurements.

TABLE 3. - Peak stress magnitude and distance into pillar rib as a function of face position (compressive strength = 1,480 psi)[1]

Face position	Left-side peak stress		Right-side peak stress	
	Magnitude, psi	Distance from left rib, ft	Magnitude, psi	Distance from right rib, ft
A.....	4,415	5.33	4,065	4.00
B.....	5,376	6.66	6,129	6.67
C.....	5,095	9.33	9,791	9.33
D.....	6,660	11.00	11,957	11.00
E.....	8,831	11.00	9,832	13.00

[1]See figure 20.

TABLE 4. - Peak stress magnitude and distance into pillar rib as a function of face position (compressive strength = 400 psi)[1]

Face position	Left-side peak stress		Right-side peak stress	
	Magnitude, psi	Distance from left rib, ft	Magnitude, psi	Distance from right rib, ft
A.....	4,227	8.00	3,965	6.67
B.....	5,059	11.00	5,870	11.00
C.....	5,082	13.00	9,041	13.00
D.....	6,236	15.00	11,125	15.00
E.....	7,988	15.00	9,635	15.00

[1]See figure 22.

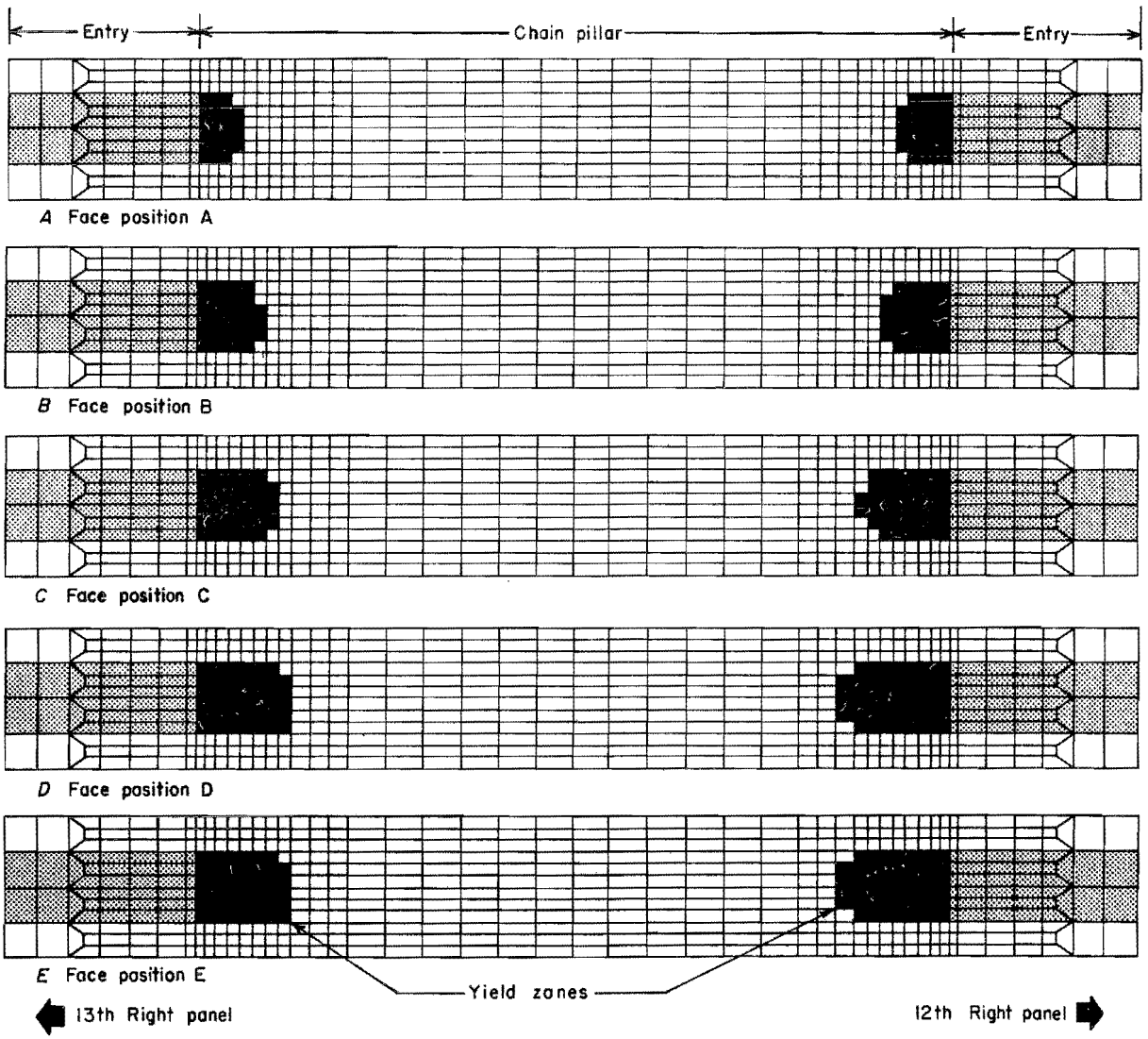

OPENING	0.01	0.01	0.03	0.05	0.10	0.25	0.55	1.00	1.00	0.40	0.15	0.05	0.05	0.03	0.01	0.01	0.01	OPENING
	0.01	0.01	0.01	0.03	0.05	0.10	0.30	0.65	0.65	0.25	0.10	0.05	0.05	0.03	0.01	0.01	0.01	
	0.01	0.01	0.01	0.03	0.05	0.05	0.20	0.50	0.50	0.20	0.10	0.05	0.05	0.01	0.01	0.01	0.01	
	0.01	0.01	0.01	0.03	0.05	0.05	0.20	0.45	0.55	0.20	0.10	0.05	0.05	0.01	0.01	0.01	0.01	
	0.01	0.01	0.01	0.03	0.05	0.05	0.25	0.60	0.70	0.30	0.15	0.05	0.05	0.03	0.01	0.01	0.01	
	0.01	0.01	0.01	0.03	0.05	0.15	0.45	0.90	1.00	0.55	0.25	0.10	0.05	0.03	0.01	0.01	0.01	

0 1 2 3 4 5 6 7
DISTANCE FROM RIB, ft

9 8 7 6 5 4 3 2 1 0
DISTANCE FROM RIB, ft

F Final computed yield factors in coal pillar for face position E

FIGURE 19.–Progressive pillar rib failure as a function of face position (compressive strength = 1,480 psi).

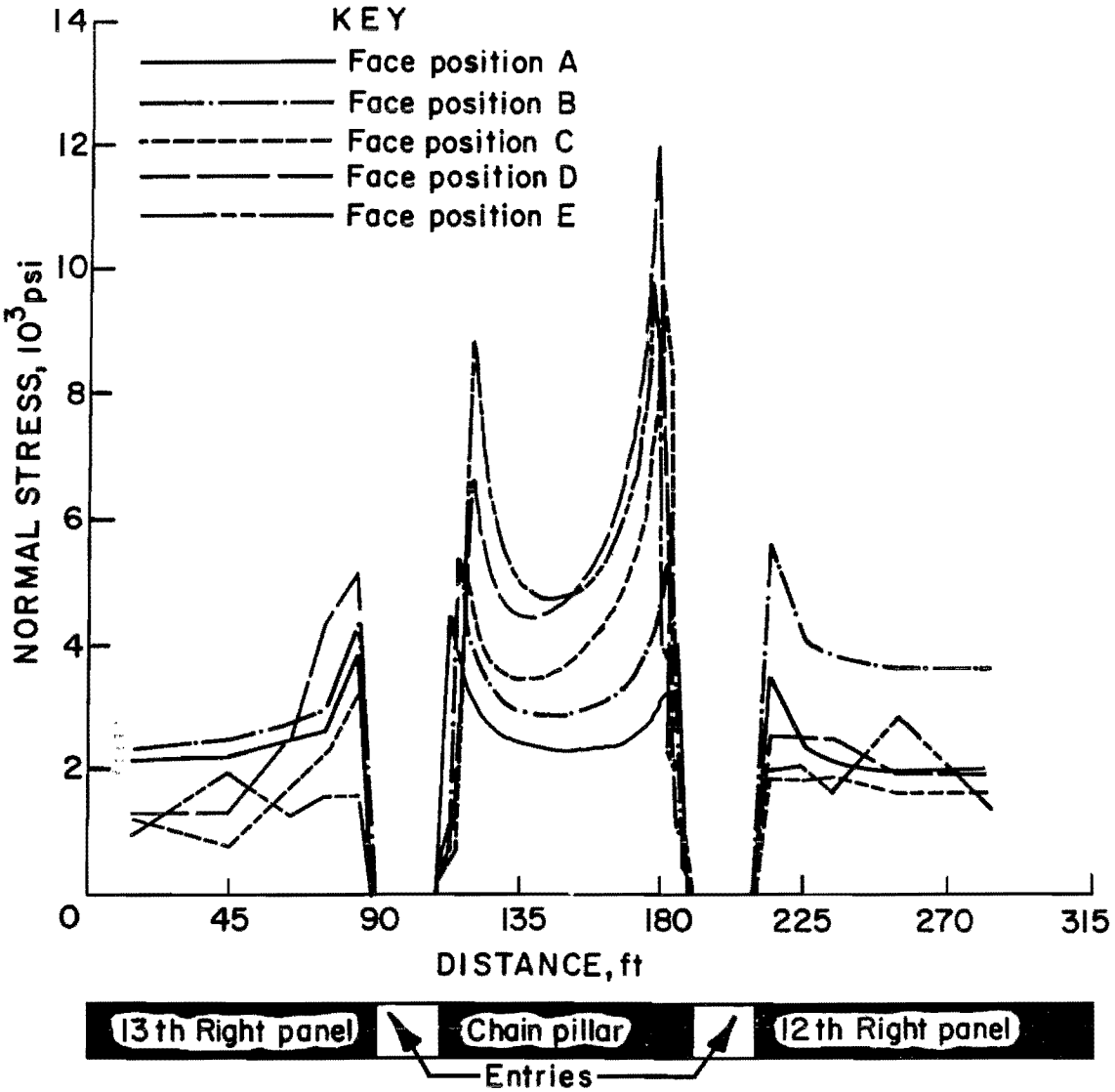

FIGURE 20.–Change in normal stress profile through pillar cross section for face positions A through E from numerical modeling analysis (compressive strength = 1,480 psi).

EFFECTS OF LOAD PATH DEPENDENCY

The effects of load path dependency on final results were investigated. In other words, is it necessary to model all of the face positions sequentially, as was illustrated in the example, and to calculate the cumulative effects of progressive failure at each face position? Or, would the same failed state be predicted by directly modeling the last face position and going through the required number of iterations for one load case to reach a final steady state of equilibrium?

In general, the same failed state can be calculated with fewer overall iterations by directly modeling the last face position. However, caution is advised for situations where the induced loading at one of the intermediate face positions generates higher stresses in the area of interest than at the last face position. A situation such as this can very easily exist if additional stress concentrations resulting from the effects of multiple seam interaction occur at an intermediate face position. In that case, the same degree and extent of progressive failure would not be predicted if only the last face position were modeled.

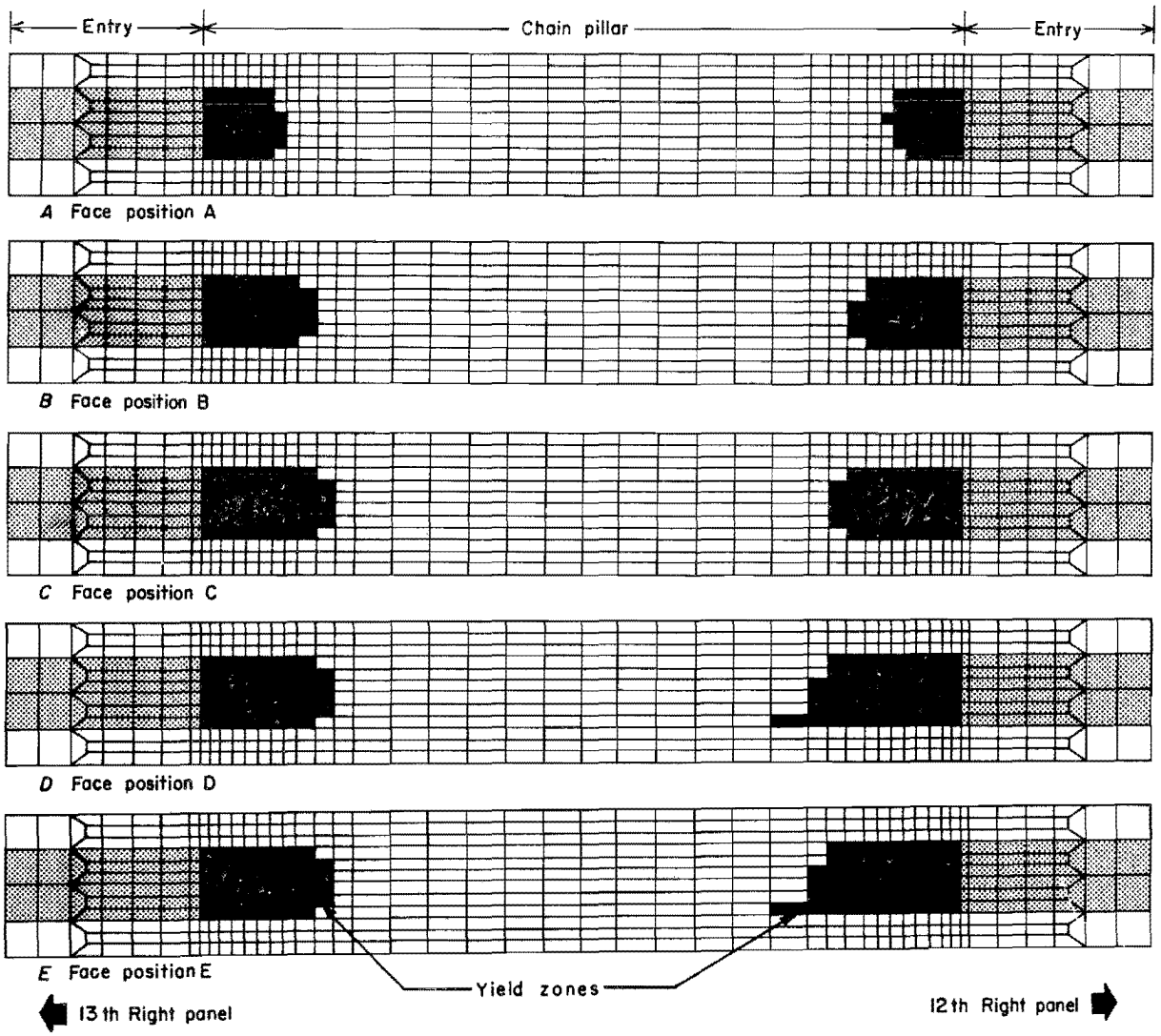

0.01	0.01	0.01	0.01	0.03	0.05	0.10	0.20	0.55	1.00	1.00
0.01	0.01	0.01	0.01	0.01	0.03	0.05	0.10	0.30	0.85	1.00
0.01	0.01	0.01	0.01	0.01	1.03	0.05	0.10	0.25	0.65	1.00
0.01	0.01	0.01	0.01	0.01	0.01	0.05	0.10	0.25	0.65	1.00
0.01	0.01	0.01	0.01	0.01	0.03	0.05	0.10	0.30	0.75	1.00
0.01	0.01	0.01	0.01	0.03	0.05	0.10	0.20	0.50	1.00	1.00

OPENING

0 2 4 6 8 10 12 14 16
DISTANCE FROM RIB, ft

1.00	1.00	0.85	0.35	0.15	0.05	0.03	0.01	0.01	0.01	0.01	0.01
1.00	1.00	1.00	0.60	0.20	0.05	0.03	0.01	0.01	0.01	0.01	0.01
1.00	0.95	0.45	0.15	0.10	0.50	0.01	0.01	0.01	0.01	0.01	0.01
1.00	0.85	0.45	0.20	0.10	0.05	0.01	0.01	0.01	0.01	0.01	0.01
1.00	0.85	0.55	0.25	0.10	0.05	0.01	0.01	0.01	0.01	0.01	0.01
0.95	0.90	0.75	0.50	0.20	0.10	0.05	0.03	0.01	0.01	0.01	0.01

OPENING

20 18 16 14 12 10 8 6 4 2 0
DISTANCE FROM RIB, ft

F Final computed yield factors in coal pillar for face position E

FIGURE 21.–Progressive pillar rib failure as a function of face position (compressive strength = 400 psi).

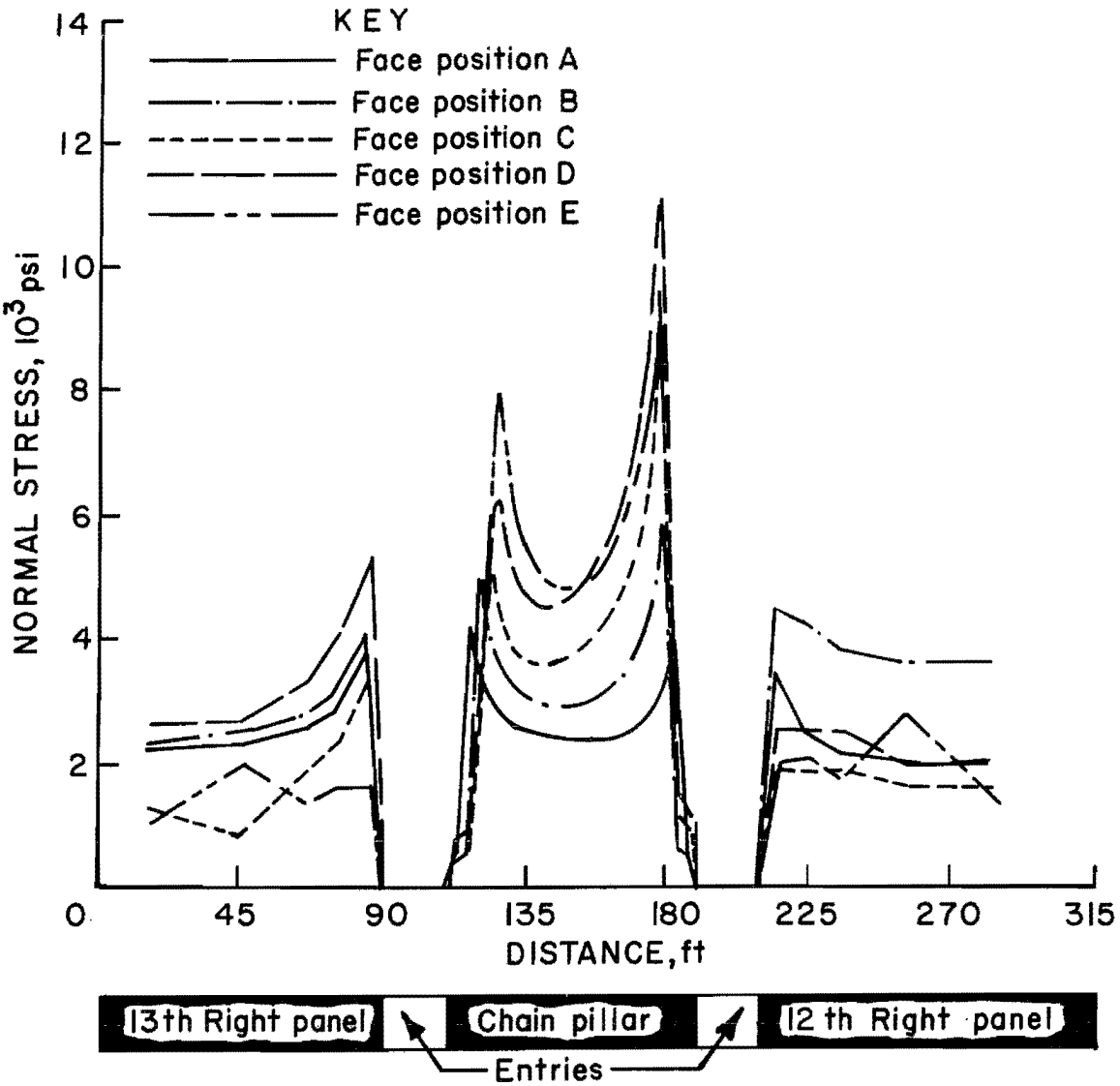

FIGURE 22.–Change in normal stress profile through pillar cross section for face positions A through E from numerical modeling analysis (compressive strength = 400 psi).

In the example problem described in this report, the intermediate overall induced loading onto the chain pillar being studied continued to increase up to face position D, so that the results obtained from directly modeling face position D compared very closely with the results from calculating the summation of progressive failure at each face position leading up to face position D. Note, however, on figure 15, that for face position E, the peak abutment stress is less than that for face position D in the rib of the chain pillar adjacent to the 12th Right panel and greater in the chain pillar rib adjacent to the 13th Right panel. The rate of growth of the yield zones is reflected accordingly. Figures 23 and 24 illustrate that the final steady-state pillar rib failure and the normal stress profile through the chain pillar cross section are path-independent for this particular situation. Twenty iterations in the finite-element model were required to arrive at the final steady state conditions from summing cumulative effects of modeling face positions A through D, whereas only 14 iterations were required to reach the same state by modeling 1 load step at face position D. This results in considerable savings of computer time and cost to conduct a comparable analysis. Face position E was not modeled independently.

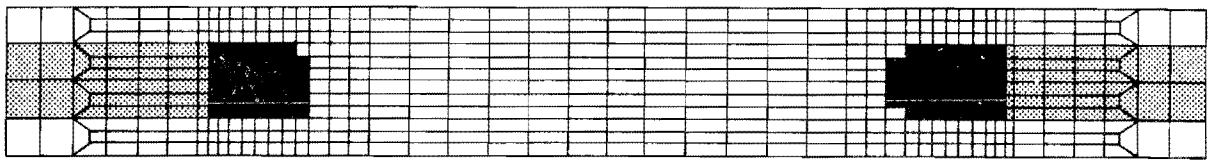

A Cumulative effect of modeling face positions A–D

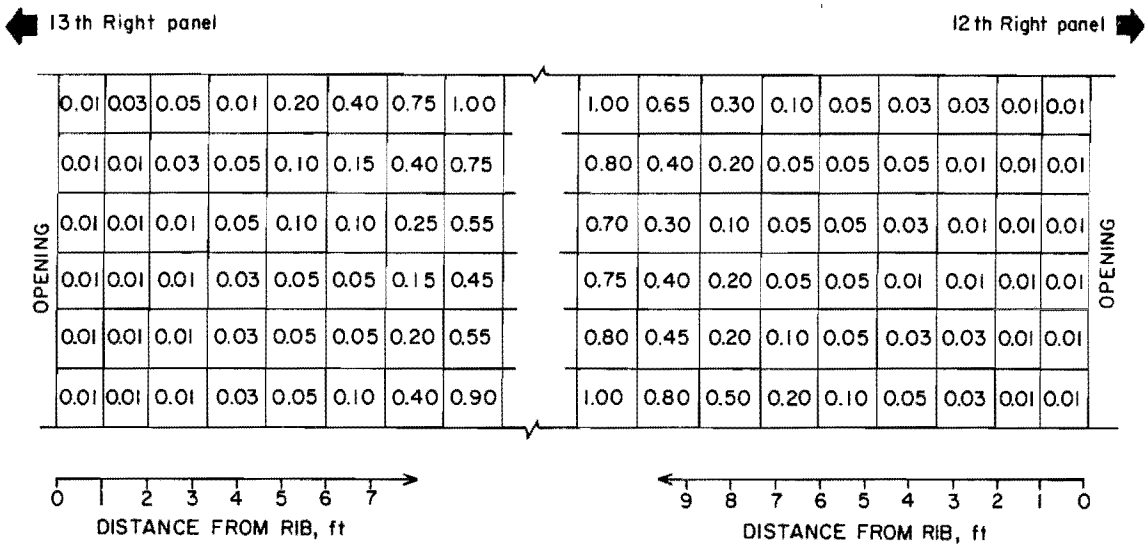

B Final computed yield factors in coal pillar modeling face positions A–D cumulatively

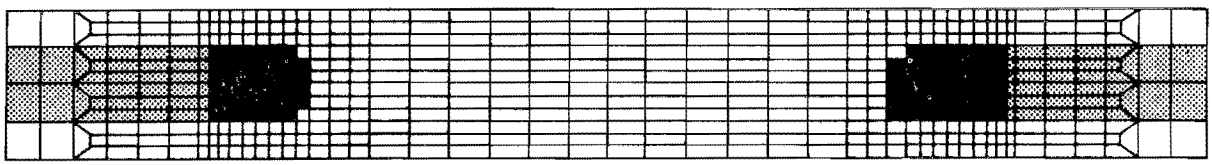

C Effect of modeling face position D directly

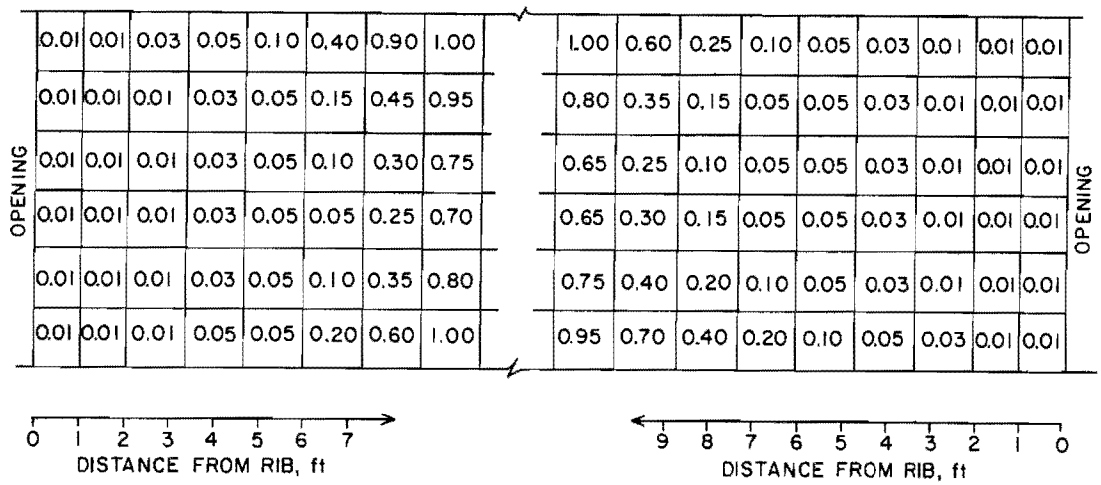

D Final computed yield factors in coal pillar modeling face position D directly

FIGURE 23.–Final steady-state pillar rib failure at face position D (compressive strength = 1,480 psi).

CONCLUSIONS

Given an expected future emphasis on extraction of multiple coal seams in close proximity, an immediate need exists to establish design criteria, guidelines, and systematic computational procedures for mine planning to minimize the ground control hazards associated with multiple-seam mining at depths below 1,500 ft. The guidelines should be based on previous mining experience, field investigations, and correlated computational analysis.

Numerical model studies can help reduce some of the uncertainties associated with seam interaction effects. The procedure proposed in the report reduces some of the complexities associated with analyzing a three-dimensional problem. A combination of the multiple-seam displacement-discontinuity method and a two-dimensional finite-element vertical cross section model can produce very refined results for an area of particular interest. The displacement-discontinuity program (MULSIM) calculates expected loadings for mine structures affected by overlying or underlying seams. Elastic finite-element analysis (ADINA), using the yield-factor approach, can help clarify the stability of coal pillars by simulating the degree and extent of progressive rib failure and subsequent load transfer.

The modeling procedure must conform to practical constraints. For example, the number and location of longwall face positions chosen for displacement-discontinuity analysis must be based on practical engineering judgement. Likewise, the number of iterations performed in a stability analysis must be held within a practical limit. Selection of model material properties should be based on all available information, but such selection depends ultimately on sound engineering judgment.

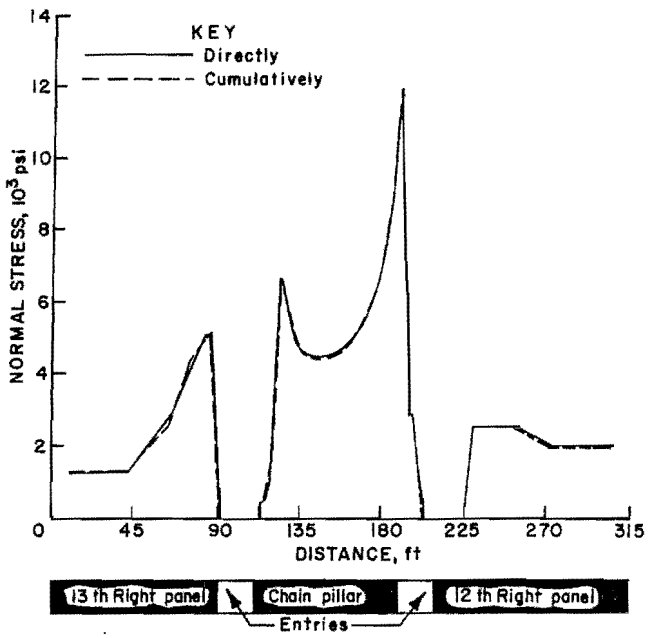

FIGURE 24.–Final normal stress profile through pillar cross section at face position D (compressive strength = 1,480 psi).

The numerical modeling results and field measurements reported here agree qualitatively with regard to the degree and extent of pillar yielding and the magnitude of stresses in the pillar. The quantitative discrepancies are attributable largely to the choice of material property values, to interpretation of experimentally determined stress, and to the analytical assumptions used. Further research will be needed to evaluate the sensitivity of pillar stability and load transfer to various material properties.

REFERENCES

1. U.S. Energy Information Agency (Dep. Energy). Annual Energy Review. DOE/EIA-0384(84), Dist. Category UC-98, Apr. 1985, 275 pp.

2. Singh, M. A., and M. F. Dunn. Investigation of Problems and Benefits of Underground Multiple Seam Mining (U.S. Dep. Energy contract DEAC-01-79ET14242, Engineers International, Inc.). Aug. 1981, 292 pp.

3. Chekan, G. J., R. J. Matetic, and J. A. Galek. A Case Study of Ground Control Problems Related to Multiple Seam Mining in the Pittsburgh and Sewickley Coalbeds. Soc. Min. Eng. AIME preprint 85-325, 1985, 9 pp.

4. Jacobi, O., and G. Everling. Practical Ground Control. Gluckauf, Essen, Federal Republic of Germany, 1976, 496 pp.

5. Pariseau, W. G. Ground Control in Multi-Level Room and Pillar Mines (grants G1105048 and G1115491, Univ. UT). BuMines OFR 150-83, 1983, 111 pp.; NTIS PB 83-252965.

6. Su, W. H., S. M. Hsiung, and S. S. Peng. Optimum Mining Plan for Multiple Seam Mining. Paper in Proceedings of the 25th U.S. Symposium on Rock Mechanics (Evanston, IL, 1984). Soc. Min. Eng. AIME, 1984, pp. 591-602.

7. Carr, F., E. Martin, and B. H. Gardner. How To Eliminate Roof and Floor Failures With Yield Pillars. Coal Min., pt. I, v. 21, Dec. 1984, pp. 62-70; pt. II, v. 22, Jan. 1985, pp. 44-51.

8. Gaddy, F. L. A Study of the Ultimate Strength of Coal as Related to the Absolute Size of the Cubical Specimen Tested. Bull. VA Polytech. Inst., Eng. Exp. Stn. Ser. 112, 1956, 27 pp.

9. Holland, C. T. The Strength of Coal in Mine Pillars. Paper in Proceedings of the 6th Symposium on Rock Mechanics (Univ. MO, Rolla, MO, 1964). Univ. MO, Rolla, 1964, pp. 450-466.

10. Hustrulid, W. A. A Review of Coal Pillar Strength Formulas. Rock Mech., v. 8, 1976, pp. 115-145.

11. Babcock, C. O., T. Morgan, and K. Haramy. Review of Pillar Design Equations Including the Effects of Constraint. Paper in Proceedings of the First Conference on Ground Control in Mining (Univ. WV, Morgantown, WV, July 27-29, 1981). Univ. WV, 1981, pp. 23-24.

12. Wilson, A. H., and D. P. Ashwin. Research Into the Determination of Pillar Size. Part I. An Hypothesis Concerning Pillar Stability. Min. Eng., (London), v. 131, June 1972, pp. 409-417.

13. Wilson, A. H. The Effect of Yield Zones on the Control of Ground. Paper in 6th International Strata Control Conference (Banff, Canada, Sept. 23-28, 1977). Can. Inst. Min. and Metall. (CIM), 1977, 21 pp.

14. Babcock, C. O. Effect of End Constraint on the Compressive Strength of Model Rock Pillars. Trans. AIME, v. 244, Dec. 1969, pp. 357-363.

15. Babcock, C. O., and D. L. Bickel. Constraint--The Missing Variable in the Coal Burst Problem. Paper in Proceedings of the 25th U.S. Symposium on Rock Mechanics (Evanston, IL, 1984). Soc. Min. Eng. AIME, 1984, pp. 539-547.

16. Babcock, C. O. Constraint Is the Prime Variable in Pillar Strength. Paper in Proceedings of Fourth Conference on Ground Control in Mining (Univ. WV, Morgantown, WV, July 22-24, 1985). Univ. WV, 1985, pp. 105-116.

17. Panek, L. Estimating Mine Pillar Strength From Compression Tests. Trans. Soc. Min. Eng. AIME, v. 268, 1980, pp. 1749-1761.

18. Serata, S., F. Carr, and E. Martin. Stress Control Method Applied to Stabilization of Underground Coal Mine Openings. Paper in Proceedings of the 25th U.S. Symposium on Rock Mechanics (Evanston, IL, 1984). Soc. Min. Eng. AIME, 1984, pp. 583-590.

19. Sinha, K. P. Displacement Discontinuity Technique for Analyzing Stresses and Displacements Due to Mining in Seam Deposits. Ph.D. Thesis, Univ. MN, Minneapolis, MN, 1979, 311 pp. Univ. Microfilms Int., Ann Arbor, MI; Facsimile No. 7918390.

20. Crouch, S. L., and C. Fairhurst. The Mechanics of Coal Mine Bumps and the Interaction Between Coal Pillars, Mine Roof, and Floor (contract H0101778, Univ. MN). BuMines OFR 53-73, 1973, 88 pp.; NTIS PB 222 898.

21. Bathe, K. J. ADINA, A Finite Element Program for Automatic Dynamic Incremental Nonlinear Analysis. MIT, Mech. Eng. Dep., Cambridge, MA, Rep. 82448-1, Sept. 1975, (rev. Dec. 1978), 435 pp.

22. Kidybinski, A., and C. O. Babcock. Stress Distribution and Rock Fracture Zones in the Roof of Longwall Face in a Coal Mine. Rock Mech., v. 5, No. 1, 1973, pp. 1-19.

23. Kripakov, N. P. Analysis of Pillar Stability on Steeply Pitching Seam Using the Finite Element Method. BuMines RI 8579, 1981, 33 pp.

24. Kripakov, N. P., and M. T. Melvin. A Computer Program To Simulate Progressive Rock Failure around Coal Mine Entries. Paper in Proceedings of the First Conference on Use of Computers in the Coal Industry (Univ. WV, Morgantown, WV, Aug. 1-3, 1983). Soc. Min. Eng. AIME, 1983, pp. 487-502.

25. Beckett, L. A., and R. S. Madrid. MULSIM/BM--A Structural Analysis Computer Program for Mine Design. BuMines IC 9168, 1988, 302 pp.

26. Crouch, S. L., and A. M. Starfield. Boundary Element Methods in Solid Mechanics. Allen & Unwin, 1983, 322 pp.

27. Salamon, M. D. G. Elastic Analysis of Displacements and Stresses Induced by the Mining of Seam or Reef Deposits, Parts I-IV. J. S. Afr. Inst. Min. and Metall., v. 64, No. 4, 1964, pp. 128-149; v. 64, No. 6, 1964, pp. 197-218; v. 64, No. 10, 1965, pp. 468-500; v. 65, No. 5, 1965, pp. 319-338.

28. Beckett, L. A., and R. S. Madrid. Practical Application of MULSIM/BM for Improved Mine Design. Paper in Use of Computers in the Coal Industry (3d Conf., Univ. WV, Morgantown, WV, July 28-30, 1986). A. A. Balkema, Rotterdam, Netherlands, 1986, pp. 209-219.

29. Bathe, K. J., E. L. Wilson, and R. H. Iding. NONSAP--A Structural Analysis Program for Static and Dynamic Response of Nonlinear Systems. Univ. CA, Berkeley, CA, Dep. Civ. Eng., Rep. USCESM 74-3, 1974, 178 pp.

30. Bathe, K. J. ADINA/BM--A General Computer Program for Nonlinear Analysis of Mine Structures (contract J0255008, MIT). BuMines OFR 19-82, 1978, 415 pp.; NTIS PB 82-180993.

31. Obert, L., and W. I. Duvall. Rock Mechanics and the Design of Structures in Rock. Wiley, 1967, 650 pp.

32. Pariseau, W. G., and I. M. Eitani. Comparisons Between Finite Element Calculations and Field Measurements of Room Closure and Pillar Stress During Retreat Mining. Int. J. Rock Mech., Min. Sci. & Geomech. Abstr., v. 18, 1981, pp. 305-319.

33. Bieniawski, Z. T. Deformational Behavior of Fractured Rock Under Multiaxial Compression. Paper in Proceedings of an International Conference on Structures, Solid Mechanics and Engineering Materials (Southhampton, England, June 20, 1969). Wiley, 1969, pp. 589-598.

34. _____. Geomechanics Classification of Rock Masses and Its Application in Tunnelling. Paper in Proceedings of the Third International Congress on Rock Mechanics (Denver, CO, 1974). Int. Soc. Rock Mech., 1974, v. 11a, 1974, pp. 27-32.

35. _____. Rock Mass Classification in Rock Engineering. Paper in Proceedings of the Symposium on Exploration for Rock Engineering (Johannesburg, Repub. S. Afr.). A. A. Balkema, Rotterdam, Netherlands, 1976, v. 1, pp. 97-106.

36. Barton, N., R. Lien, and J. Lunde. Engineering Classification of Rock Masses for the Design of Tunnel Support. Rock Mech., v. 6, No. 4, 1974, pp. 189-236. Originally publ. as Analysis of Rock Mass Quality and Support Practice in Tunnelling. Norwegian Geotech. Inst. Rep. 54206, June 1974, 74 pp.

37. Hoek, E., and E. T. Brown. Underground Excavations in Rock. Inst. Min. and Metall., London, 1980, 527 pp.

38. Bieniawski, Z. T. Determining Rock Mass Deformability: Experience From Case Histories. Int. J. Rock Mech., Min. Sci. & Geomech. Abstr., v. 15, 1978, pp. 237-247.

39. Hardy, M. P., and J. F. T. Agapito. Pillar Design in Underground Oil Shale Mines. Paper in Design Methods in Rock Mechanics, ed. by C. Fairhurst and S. L. Crouch (16th U.S. Symp. on Rock Mechanics). ASCE, 1975.

40. Hardy, M. P., K. E. Matthews, and C. M. St. John. Geotechnical Assessment of Potential Methods of Underground Mining of the Copper-Nickel Deposits of Northeastern Minnesota (contract H0272006, Univ. MN). BuMines OFR 62-79, 1978, 91 pp.

41. St. John, C. M., M. Christianson, and D. L. Peterson. Evaluation of Mine Parameters for Copper-Nickel Deposits of Northern Minnesota (contract J0295003, Univ. MN). BuMines OFR 10-80, Feb. 1979, 109 pp.; NTIS PB 80-144074.

42. Salamon, M. D. G. Reconsolidation of Caved Areas. Collieries Res. Lab., Transvaal and Orange Free State Chamber of Mines Res. Org., Repub. S. Afr. Res. Rep. 58/66, July 1966, 25 pp.

43. Mozumdar, B. J. A Mathematical Model of Ground Movement Due to Underground Mining. Ph.D. Thesis, PA State Univ., State College, PA, 134 pp. Univ. Microfilms, Ann Arbor, MI, Facsimile No. 75-9815.

44. Kripakov, N. P., L. A. Beckett, and D. A. Donato. Loading on Underground Mine Structures Influenced by Multiple Seam Interaction. Paper in International Symposium on Application of Rock Characterization Techniques in Mine Design (SME-AIME Annu. Meet., New Orleans, LA, Mar. 1986). Soc. Min. Eng., AIME, 1986, pp. 225-236.

45. Peng, S. S. Coal Mine Ground Control. Wiley, 1978, 491 pp.

46. Lu, P. H. Determination of Ground Pressure Existing in a Visco-elastic Rock Mass by Use of Hydraulic Borehole Pressure Cells. Paper in Proceedings of the International Symposium on Weak Rock (Tokyo, Japan, Sept. 1981). A. A. Balkema, Rotterdam, Netherlands, 1981, v. 1, pp. 459-465.

47. _____. Mining Induced Measurement With Hydraulic Borehole Pressure Cells. Paper in Proceedings of the 25th U.S. Symposium on Rock Mechanics (Evanston, IL, 1984). Soc. Min. Eng. AIME, 1984, pp. 204-211.

48. Babcock, C. O. Equations for the Analysis of Borehole Pressure Cell Data. Paper in Proceedings of the 27th Rock Mechanics Symposium (Univ. AL, Tuscaloosa, AL, June 23-25, 1986). Soc. Min. Eng. AIME, 1986, pp. 233-240.

APPENDIX.--ENGINEERING SYMBOLS USED IN THIS REPORT

A	unit area, in^2
C	uniaxial unconfined compressive strength, psi
c	gob convergence, ft
C_f	effective uniaxial compressive strength, psi
C_o	original uniaxial compressive strength, psi
E_g	secant elastic gob modulus, psi
E_{GA}	elastic gob modulus, ADINA model, psi
E_{GM}	elastic gob modulus, MULSIM model, psi
E_f	effective Young's modulus, psi
E_m	modulus of deformation
E_o	original Young's modulus, psi
F	force, lb
g	in situ gob zone height, ft
IP	integration point
K	spring stiffness, lb/in
k'	material constant, psi
K_{GA}	gob stiffness, ADINA model, lb/in
K_{GM}	gob stiffness, MULSIM model, lb/in
l	length of one dimensional truss member, in
Ln	natural log function
m	seam height, ft
P	equilibrium point for gob
p	stress carried by gob, psi
Q	tunneling quality index, unitless
RMR	rock-mass rating, unitless
S_r	height-to-width ratio of rock mass representative volume, ft/ft
SF	safety factor, psi/psi
SF_τ	safety factor at iteration τ, psi/psi
S_L	height-to-width ratio of laboratory sample, ft/ft

S_o	cohesion, psi
T	tensile strength, psi
$\tan\beta$	$(1 + \sin\phi)/(1 - \sin\phi)$, unitless
V_c	rock mass representative volume, ft^3
V_L	volume of laboratory rock sample, ft^3
w	amount of gob zone main-roof-to-floor convergence, ft
YF	yield factor, unitless
α	volume reduction factor, unitless
β	shape reduction factor, unitless
δ	displacement, in
ε_g	strain sustained by gob, in/in
ε_{max}	maximum possible gob strain, in/in
ε_o	equilibrium strain for gob, in/in
θ	failure plane angle = $45° + \phi/2$, deg
ν_f	effective Possion's ratio, psi/psi
ν_o	original Poisson's ratio, psi/psi
σ_A	applied stress, psi
σ_c	confining stress, psi
σ_F	compressive failure stress (Mohr-Coulomb strength), psi
σ_g	stress sustained by gob (linear equation), psi
σ_L	laboratory strength, psi
σ_{max}	maximum compressive principal stress, psi
σ_{min}	minimum compressive principal stress, psi
σ_n	applied normal stress, psi
σ_{NL}	stress sustained by gob (nonlinear equation), psi
σ_o	virgin overburden stress, psi
σ_R	reduced strength, psi
σ_T	applied tensile stress, psi
τ_F	shear failure stress, psi
τ_n	applied shear stress, psi
ϕ	angle of internal friction, deg

U.S. GOVERNMENT PRINTING OFFICE: 1988 — 547-000/80,042

INT.-BU.OF MINES,PGH.,PA. 28725